Improved Trial Wave Functions for Quantum Monte Carlo Calculations of Nuclear Systems and Their Applications

Cody L. Petrie

March 11, 2019

Outline and Due Dates

Also add a list of figures???
Oliver will probably want to see pictures of scalings and timings. Scaling/processor etc. Include some nice pictures of these things.

1. Background/Motivation Tuesday Feb 19 Hardest section but really important. Make sure to explain why the stuff we're working on is interesting, this will lead into talking about other methods.
   (a) Other methods like HF and no-core shell model
   (b) General outline of the dissertation
2. Quantum Monte Carlo Friday Feb 22
   (a) VMC
   (b) DMC
   (c) AFDMC
      i. Mixed expectation values, operator breakup
   (d) Hamiltonian - Phenomenogolical + χEFT + some results with AFDMC/GFMC
3. Trial Wave Function Friday Feb 15
   (a) Slater Determinants
   (b) Pfaffian Explain what it's used for (superfluidity etc.) and why it's more efficient than the SD stuff (need many thousands of SD's to do the same thing).
   (c) Spin-Isospin Dependent Correlations
      i. Quadratic Correlations - include results
         A. Results
      ii. Exponential correlations . . . why they aren't working or how to do it, cluster decomposition If not working then don't say much about it. Explain that there are large variances that need to be taken care of etc.

(d) Alessandro's wave function with T^2 fix attempts. Maybe . . . maybe don't include

4. Alpha-clustering Friday Mar 1

   (a) Theory

   (b) Results

5. Conclusion Friday Mar 8

   (a) Future Work

Make sure to include stuff for each member of the committee.

1 Background and Motivation

Nuclear physics sheds light on the extremes. From the structure and processes of atomic nuclei and hypernuclei to the formation and structure of some of the largest objects in the universe, neutron stars. One of the largest obstacles to these regimes comes from our incomplete knowledge of the nuclear interaction. Once a possible interaction is selected, the next obstacle is to solve for properties of many-body nuclear systems using the selected, and often complicated, interaction. Currently the popular choices for 2- and 3-body nuclear interactions come in two flavors, phenomenological and those based in Chiral Effective Field Theory (χEFT). There are a large number of methods that have been developed to solve the many-body nuclear problem, and I will be using the Auxiliary Field Diffusion Monte Carlo (AFDMC) method. One of the early methods used in nuclear physics is the Hartree-Fock (HF) method. The HF method has been used to study condensed matter systems for most of a decade [1, 2, 3], but wasn't used in nuclear physics until much later when the understanding of the nuclear interaction was improved [4, 5]. HF begins with the mean field approximation which accounts for all inter-particle interactions by some average interaction. The wave function is usually assumed to be a Slater determinant, which is varied to minimize the energy. These calculations are often the starting place for other more sophisticated calculations. Such is the case with AFDMC and other Quantum Monte Carlo (QMC) methods.

Other notable methods are the basis set methods such as no core shell model [6, 7], the coupled-cluster method [8], and the self-consistent Green's function method [9, 10]. For these methods the wave function of the nuclear system is written in terms of a truncated basis, often a harmonic oscillator basis. The momentum cutoff of the basis needs to be higher than the important momenta of the interaction that is being used, in order to do calculations in momentum space. This means however that calculations with sharp potentials, like local hard wall potentials, are difficult to do with basis set methods due to the relatively high momenta needed to describe such potentials. They do employ techniques such as Similarity Renormalization Group [11] to soften these types of interaction, which consists of applying a regulator that will smoothly cut off the high momentum dependence of hard interactions such as the local contact interaction. This allows them to decrease the number of basis functions needed to describe the system accurately. One of the advantages of basis set methods is that they can use local and non-local, i.e. velocity dependent, potentials. Quantum Monte Carlo (QMC) methods, which I am using in this work, complement these basis set methods. QMC

methods are currently limited to mostly local potentials[1] [12], but can converge for a wide variety of local Hamiltonians. Also, QMC methods do not have the momentum cutoff limits or the poor scaling with basis set size of the basis set methods.

One of the most accurate QMC methods is the Green's Function Monte Carlo (GFMC) method, which has had good success calculating properties of light nuclei and nuclear matter using 2- and 3-body potentials as well as electroweak currents [13]. GFMC has been used to calculate binding energies as well as excitation spectra for nuclei up to ^{12}C with good accuracy. GFMC has also been used to study electroweak current, elastic and inelastic form

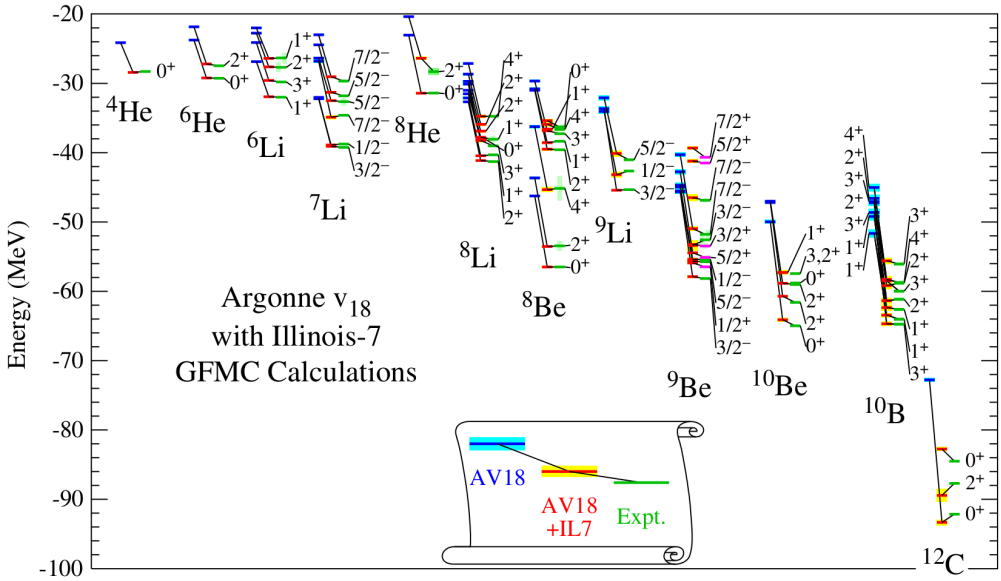

Figure 1: Ground and excited state energies calculated with GFMC calculated with the AV18 and AV18+IL7 potentials compared to experiment. Figure taken from [13].

factors, and the neutron and symmetric nuclear matter equation of state (EOS) which have been used to study the structure of neutron stars. Nuclear calculations using the GFMC method are limited due to the explicit sum over spin states when calculating expectation values, which grows exponentially with the number of nucleons. The number of spin-isospin states for a system with A nucleons and Z protons is

$$\frac{A!}{Z!(A-Z)!}2^A \tag{1}$$

In 1999 Schmidt and Fantoni [14] proposed the AFDMC method which is practically identical to GFMC in its Monte Carlo sampling of spatial integrals, however AFDMC uses Monte Carlo to sample the spin-isospin sums as well. Since then AFDMC has been used to study light nuclei up to ^{40}Ca [15, 16], neutron stars [17, 18, 19], the hyperon puzzle [20, 21], as well as neutron and nuclear matter equation of states [22, 23, 19], with both phenomenological interactions and interactions based on Chiral Effective Field Theory (χEFT) [24, 25] with 2- and 3- body forces. For recent reviews of QMC methods I refer the reader to [13, 26].

[1]Currently, interactions that are linear in the momentum can be used. Higher order terms are treated perturbatively.

In this study, for simplicity, I have only used the AV6' phenomenological potential which is a refitting of the full Argonne $v18$ (AV18) [27] to only the first 6 operators, $(1, \boldsymbol{\sigma}_i \cdot \boldsymbol{\sigma}_j, S_{ij}) \otimes (1, \boldsymbol{\tau}_i \cdot \boldsymbol{\tau}_j)$, where the tensor term is $S_{ij} = 3\boldsymbol{\sigma}_i \cdot \hat{r}_{ij} \boldsymbol{\sigma}_j \cdot \hat{r}_{ij} - \boldsymbol{\sigma}_i \cdot \boldsymbol{\sigma}_j$. There has been much success with these phenomenological NN AV18 and 3N Urbana [28] and Illinois potentials [29]. However, phenomenological potentials have few connections to the underlying theory of QCD. Potentials based on χEFT have been developed in the past [30], but for some time they were only cast in momentum space or in a non-local form in position space, neither of which can be used with QMC. Recently the non-localities have been removed from the position space potentials up to next-to-next-to leading order (N2LO) in the chiral expansion and many AFDMC calculations have been done using these new potentials [31].

The goal of this study is to develop improved trial wave functions to be used with the AFDMC method. AFDMC was developed to extend the success of GFMC to larger systems. However, to calculate properties of larger systems accurately, better trial wave functions are needed. I will discuss the extension of these improved wave functions to some physical systems. The structure of this dissertation will be as follows.

In chapter 2, I will give an overview of the relevant QMC methods such as Variational Monte Carlo (VMC), Diffusion Monte Carlo (DMC), and AFDMC. I will also discuss the Hamiltonians used. Though I have only used phenomenological potentials in this work, an obvious extension to this work would be to apply these improved wave functions to the newly developed χEFT interactions, and so I will give a brief overview of those interactions as well.

In chapter 3, I will discuss the trial wave function. I will start by discussing the properties that we expect a good nuclear wave function to have and then I will introduce the most basic wave functions that satisfy these properties and are used as building blocks for many QMC and other calculations. I will then proceed to describe possible improvements to the existing wave functions and I will describe the specific improvements I have made as part of this work.

In chapter 4, I will extend the improved trial wave function to study the formation of alpha particles in neutron star crusts. I will show how important the improvements to the trial wave function are for describing correlated systems. In chapter 5 I will conclude and suggest possible extensions to the work that I have described.

2 Quantum Monte Carlo

Many problems in nuclear physics involve a large number of particles in addition to a complicated interparticle interaction. The Schrödinger equation used to solve these problems involves a large dimensional integral with a complicated integrand. This is unfeasible to solve using standard numerical methods. Quantum Monte Carlo was designed to tackle these problems by sampling the large dimensional integrals in a way that reduces the necessary computation while still converging to an accurate answer. With an infinite number of samples QMC calculations are exact, but with a sufficiently large number of samples the integrals can converge with controlled statistical errors. Two main ingredients to these QMC methods are Monte Carlo integration and the Metropolis algorithm. I will first describe these two techniques after which I will describe the QMC methods used in this work. I will then conclude by describing the Hamiltonians used with these methods.

2.1 Monte Carlo Integration

Solving for properties of many-body quantum systems often involves solving a large dimensional integral such as

$$I = \int g(\mathbf{R}) d\mathbf{R}, \tag{2}$$

where the $\mathbf{R} = \mathbf{r}_1, \mathbf{r}_2, \ldots, \mathbf{r}_N$ could be the positions of each particle in the system. Monte Carlo integration involves writing this integral in terms of a probability distribution called the importance function $P(\mathbf{R})$,

$$I = \int f(\mathbf{R}) P(\mathbf{R}) d\mathbf{R}, \tag{3}$$

where $f(\mathbf{R}) = g(\mathbf{R})/P(\mathbf{R})$. This integral is defined to be the expectation value of $f(\mathbf{R})$ with respect to the importance function $P(\mathbf{R})$. The expectation value can also be determined by averaging an infinite number of $f(\mathbf{R}_n)$ where $\mathbf{R}_n$ are sampled directly from the importance function $P(\mathbf{R})$.

$$I \equiv \langle f \rangle = \lim_{N \to \infty} \frac{1}{N} \sum_{n=1}^{N} f(\mathbf{R}_n) \tag{4}$$

This expectation value can be approximated by averaging over a sufficiently large number of samples

$$I \approx \frac{1}{N} \sum_{n=1}^{N} f(\mathbf{R}_n), \tag{5}$$

where the statistical uncertainties can be estimated in the usual way

$$\sigma_I = \sqrt{\frac{\langle f^2 \rangle - \langle f \rangle^2}{N}} \approx \sqrt{\frac{\left(\frac{1}{N} \sum_{n=1}^{N} f^2(\mathbf{R}_n) \right) - \left(\frac{1}{N} \sum_{n=1}^{N} f(\mathbf{R}_n) \right)^2}{N-1}}. \tag{6}$$

The scaling is independent of the dimension, and thus this method is useful especially when the dimensions of the integration become large. In many-body quantum mechanics the dimension of the integrals can be quite large, including several dimensions for each particle in the calculation. Monte Carlo integration only needs to sample each of these dimensions, decreasing the work required by a substantial amount for large dimensional integrals.

2.2 Metropolis Algorithm

Monte Carlo integration requires the sampling of the importance function, $P(\mathbf{R})$. This is straight forward only for functions that have a readily invertible cumulative distribution function, $F^{-1}(\mathbf{R})$, which is not the case in our application. For the one dimensional case where $F^{-1}(\mathbf{R})$ is known, a random variables x could be sampled by drawing a random variable u from a uniform distribution from 0 to 1, which is then used as the argument of the inverse cumulative distribution function, $x = F^{-1}(u)$. The Metropolis algorithm provides a way to sample non-invertible probability distributions. The Metropolis algorithm is a

Markov chain method that generates sequential samples of a probability distribution based on the previous sample alone, and not any other previous history. These are the steps to the algorithm.

1. Start at a random position, $\mathbf{R}$.

2. Propose a move to a new position $\mathbf{R}'$, pulled from a distribution $T(\mathbf{R}'|\mathbf{R})$. T could be, for example, a Gaussian centered on the current position, but could be optimized for efficiency.

3. The probability of accepting the move is given by enforcing a detailed balance condition.

$$A(\mathbf{R}'|\mathbf{R}) = \min\left(1, \frac{P(\mathbf{R}')T(\mathbf{R}|\mathbf{R}')}{P(\mathbf{R})T(\mathbf{R}'|\mathbf{R})}\right) \tag{7}$$

4. A random number, u, is generated from a uniform distribution between 0 and 1, and the move is accepted if $A \geq u$.

There are two conditions that need to be met to guarantee that this algorithm converges to the desired distribution. First, the transitions must be able to get from any allowed state to another in a finite number of steps. Second, the algorithm cannot include cycles between the same states. This second condition is guaranteed if there is a probability to reject transitions.

2.3 Variational Monte Carlo

Variational Monte Carlo starts with a trial wave function, ψ_T, that should have some non-zero overlap with the actual ground-state wave function, and a Hamiltonian, H. The trial wave function can be written as an expansion in the basis functions of the Hamiltonian, and will often include contributions from excited states of the system.

$$\Psi_T(\mathbf{R}) = c_0\Psi_0(\mathbf{R}) + \sum_n c_n\Psi_n(\mathbf{R}) \tag{8}$$

The expectation value of the Hamiltonian in the trial state gives what is called the variational energy. Due to the overlap with excited states the variational principle guarantees that the variational energy will be an upper bound to the true ground-state wave function.

$$E_V = \frac{\int \psi_T^*(\mathbf{R})H\psi_T(\mathbf{R})d\mathbf{R}}{\int \psi_T^*(\mathbf{R})\psi_T(\mathbf{R})d\mathbf{R}} \geq E_0 \tag{9}$$

This integral is calculated using Monte Carlo integration and so it needs to be rewritten to match the form of Equation 4. One way to get it into this form is to multiply the top integrand by $\psi_T(\mathbf{R})\psi_T^{-1}(\mathbf{R})$ which gives

$$E_V = \int P(\mathbf{R})E_L(\mathbf{R})d\mathbf{R}, \tag{10}$$

where

$$P(\mathbf{R}) = |\Psi_T(\mathbf{R})|^2 / \int |\Psi_T(\mathbf{R})|^2 d\mathbf{R}, \tag{11}$$

$$E_L(\mathbf{R}) = \frac{\Psi_T^*(\mathbf{R}) H \Psi_T(\mathbf{R})}{\Psi_T^*(\mathbf{R})\Psi_T(\mathbf{R})}, \tag{12}$$

are the importance function and local energy respectively.

Using the metropolis algorithm, a set of random configurations, $\{\mathbf{R}_n : n = 1, N\}$, can be drawn from the probability distribution $P(\mathbf{R})$ and used to sample the local energy. These random configurations are called walkers and contain the positions and often the spins and isospins of each particle. The variational energy and corresponding statistical error are then given by,

$$E_V \approx \frac{1}{N} \sum_{n=1}^{N} E_L(\mathbf{R}_n), \tag{13}$$

$$\sigma_{E_V} = \sqrt{\frac{\langle E_L^2 \rangle - \langle E_L \rangle^2}{N}} \approx \sqrt{\frac{\left(\frac{1}{N} \sum_{n=1}^{N} E_L^2(\mathbf{R}_n) \right) - \left(\frac{1}{N} \sum_{n=1}^{N} E_L(\mathbf{R}_n) \right)^2}{N-1}} \tag{14}$$

Once evaluated the variational energy will be an upper bound to the ground state energy of the system. The $\Psi_T(\mathbf{R})$ is written in terms of variational parameters which are varied to minimize the variational energy. A minimum in the energy will be produced when $\Psi_T \to \Psi_0$. It is important to note however that the trial wave functions that we often use are not exactly the ground-state wave functions and so the energies that we produce are only the minimum energy for that specific trial wave function. As such, it is important to start with the best trial wave function possible. Also, this algorithm can converge to an incorrect local minimum, and so it is again important to start with a good initial trial wave function.

2.4 Diffusion Monte Carlo

Diffusion Monte Carlo (DMC) solves for the ground-state by letting the walkers diffuse in imaginary time. The Schrödinger equation

$$H\Psi = i\hbar \frac{\partial \Psi}{\partial t}, \tag{15}$$

can be written in terms of the imaginary time by substituting $\tau = it/\hbar$. The resulting equation is a diffusion equation,

$$H\Psi = -\frac{\partial \Psi}{\partial \tau}, \tag{16}$$

where the wave function Ψ is diffused with respect to τ. By separating variables we can write the solution as eigenfunctions in spatial coordinates times an exponential in imaginary time where the energies have been shifted by a parameter, E_0 in order to control the normalization, $V \to V - E_0$ and $E_n \to E_n - E_0$.

$$\Psi(\mathbf{R}, \tau) = \sum_{n=0}^{\infty} c_n \phi_n(\mathbf{R}) e^{-\tau(E_n - E_0)} \tag{17}$$

As the imaginary time grows the states with higher energy than the ground-state are exponentially damped. The parameter E_0 is adjusted to be close to the ground state energy, and thus any states with higher energy have a non-zero difference $E_n - E_0$ in the negative exponential. Thus as $\tau \to \infty$ only the ground-state remains,

$$\lim_{\tau\to\infty} \Psi(\mathbf{R},\tau) = c_0\phi_0(\mathbf{R}). \tag{18}$$

The limit, $\lim_{\tau\to\infty} \Psi(\mathbf{R},\tau) = \lim_{\tau\to\infty} e^{-(H-E_0)\tau}\Psi(\mathbf{R})$, cannot be computed directly and so the propagator is split into small steps in imaginary time. A complete set of states are inserted between the propagator and the wave function.

$$\langle \mathbf{R}'|\Psi_T(\tau)\rangle = \int d\mathbf{R}\, \langle \mathbf{R}'|\, e^{-(H-E_0)\tau}\, |\mathbf{R}\rangle\, \langle \mathbf{R}|\Psi_T(0)\rangle \tag{19}$$

The propagator is broken up into N short time propagators, $\Delta\tau = \tau/N$, and a complete set of states is inserted between each finite time propagator,

$$\begin{aligned}\langle \mathbf{R}_N|\Psi_T(\tau)\rangle = \int d\mathbf{R}_0 \ldots d\mathbf{R}_{N-1}\, \langle \mathbf{R}_N|\, e^{-(H-E_0)\Delta\tau}\, |\mathbf{R}_{N-1}\rangle \times \ldots \\ \times \langle \mathbf{R}_1|\, e^{-(H-E_0)\Delta\tau}\, |\mathbf{R}_0\rangle\, \langle \mathbf{R}_0|\Psi_t(0)\rangle\,,\end{aligned} \tag{20}$$

where $\mathbf{R}_N = \mathbf{R}'$ and $\mathbf{R}_0 = \mathbf{R}$. This can be written more conveniently in the form

$$\langle \mathbf{R}_N|\Psi_T(\tau)\rangle = \int d\mathbf{R}_0 \ldots d\mathbf{R}_{N-1} \left[\prod_{i=1}^{N} \langle \mathbf{R}_i|\, e^{-(H-E_0)\Delta\tau}\, |\mathbf{R}_{i-1}\rangle\right] \langle \mathbf{R}_0|\Psi_t(0)\rangle \tag{21}$$

$$= \int d\mathbf{R}_0 \ldots d\mathbf{R}_{N-1} \left[\prod_{i=1}^{N} G(\mathbf{R}_i, \mathbf{R}_{i-1}, \Delta\tau)\right] \langle \mathbf{R}_0|\Psi_t(0)\rangle\,, \tag{22}$$

where $G(\mathbf{R}', \mathbf{R}, \tau) = \langle \mathbf{R}'|\, e^{-(H-E_0)\tau}\, |\mathbf{R}\rangle$, is often called the Green's function or the propagator. We cannot calculate the Green's function directly and so the kinetic and potential terms need to be broken up and calculated separately.

$$G(\mathbf{R}', \mathbf{R}, \Delta\tau) = \langle \mathbf{R}'|\, e^{-T\Delta\tau} e^{-(V-E_0)\Delta\tau}\, |\mathbf{R}\rangle \tag{23}$$

This breakup is only accurate to $\mathcal{O}(\Delta\tau^2)$. With the use of the Trotter-Suzuki formula,

$$e^{-\tau\left(\hat{A}+\hat{B}\right)} = e^{-\tau\hat{B}/2)} e^{-\tau\hat{A})} e^{-\tau\hat{B}/2)} + \mathcal{O}(\tau^3) \tag{24}$$

the finite-time propagator can be written as

$$G(\mathbf{R}', \mathbf{R}, \Delta\tau) = \langle \mathbf{R}'|\, e^{-(V-E_0)\Delta\tau/2} e^{-T\Delta\tau} e^{-(V-E_0)\Delta\tau/2}\, |\mathbf{R}\rangle \tag{25}$$

$$= e^{(V(\mathbf{R}')+V(\mathbf{R})-2E_0)\Delta\tau/2}\, \langle \mathbf{R}'|\, e^{-T\Delta\tau}\, |\mathbf{R}\rangle\,. \tag{26}$$

This break up is equal to the original Green's function up to $\mathcal{O}(\Delta\tau^3)$. To minimize time step errors the step in imaginary time needs to be kept small.

The kinetic term is used to move the walkers and the potential term is used to speed up convergence via a branching algorithm. The kinetic term is given by

$$G_0(\mathbf{R}', \mathbf{R}, \Delta\tau) = \langle \mathbf{R}' | \, e^{-T\Delta\tau} \, | \mathbf{R} \rangle \,, \tag{27}$$

which can be written as a diffusion term

$$G_0(\mathbf{R}', \mathbf{R}, \Delta\tau) = \Big(\frac{m}{2\pi\hbar^2\Delta\tau} \Big)^{3A/2} e^{-m(\mathbf{R}'-\mathbf{R})^2/2\hbar^2\Delta\tau}, \tag{28}$$

where A is the total number of nucleons. The piece that contains the potential is used to give a weight which is used with the branching algorithm,

$$w(\mathbf{R}') = e^{(V(\mathbf{R}')+V(\mathbf{R})-2E_0)\Delta\tau/2}. \tag{29}$$

There are various ways to do the branch algorithm, however the simplest way is to make copies of each walker, where the number of copies for each walker that continues in the calculation is given by $\mathrm{int}(w(\mathbf{R}') + \xi)$, where ξ is a uniform random number from $[0, 1]$. This way walkers with a small weight will more often be removed from the calculation and walkers with high weights will multiply.

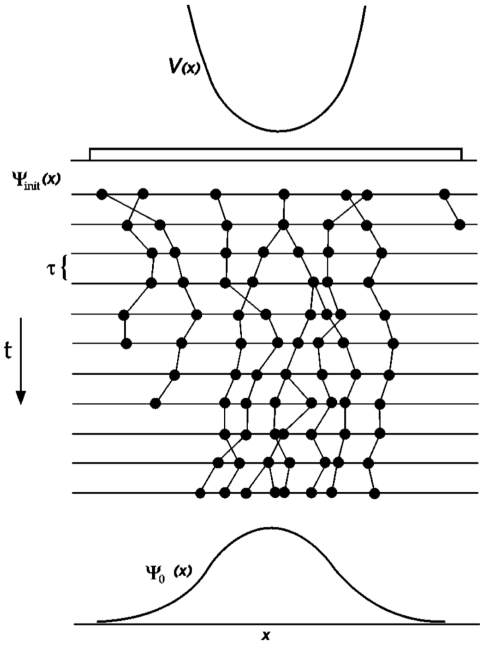

Figure 2: Diagram describing the branching algorithm for Diffusion Monte Carlo (DMC). In this 1D example a particle is confined by the potential $V(x)$ and the trial wave function $\Psi_{\mathrm{init}}(x)$ is propagated until it converges to the ground state wave function $\Psi_0(x)$. This diagram is from [32].

This sampling can have large uncertainties due to possible divergences in the branching weight in equation 29 as a result of particles getting too close or even coinciding. With the use of an importance function, $\Psi_I(\mathbf{R})$ these fluctuations can be controlled without effecting

the energy result. The importance function is used to bias the walker distributions toward $f(\mathbf{R},t) = \Psi_T(\mathbf{R},t)\Psi_I(\mathbf{R})$ instead of $\Psi_T(\mathbf{R},t)$ which effectively keeps the walkers away from locations where $|\Psi_T(\mathbf{R},t)|^2$ is small.

This can be seen by multiplying Equation 16 by $\Psi_I(\mathbf{R})$ and rewriting it in terms of $f(\mathbf{R})$ as

$$-\frac{1}{2}\nabla^2 f(\mathbf{R},t) + \nabla\cdot[\mathbf{v}_D(\mathbf{R})f(\mathbf{R},t)] + [E_L(\mathbf{R}) - E_0]\, f(\mathbf{R},t) = -\frac{\partial}{\partial t} f(\mathbf{R},t), \tag{30}$$

where $\mathbf{v}_D(R)$ is the drift velocity, defined as

$$\mathbf{v}_D(\mathbf{R}) = \Psi_I(\mathbf{R})^{-1}\nabla\Psi_I(\mathbf{R}) = \nabla \ln|\Psi_I(\mathbf{R})|\,. \tag{31}$$

The drift velocity is responsible for pushing walkers away from areas of low $|\Psi_T(\mathbf{R},t)|^2$. In practice the importance function is accounted for by directly sampling from

$$G(\mathbf{R}',\mathbf{R},\Delta\tau)\frac{\langle\mathbf{R}|\Psi_I\rangle}{\langle\mathbf{R}'|\Psi_I\rangle} \tag{32}$$

instead of from the Green's function.

It is difficult to operate through the Green's function and so often observables are computed via mixed expectation values.

$$\langle\mathcal{O}(\tau)\rangle \,\text{mixed} = \frac{\langle\Psi(\tau)|\,\mathcal{O}\,|\Psi_T\rangle}{\langle\Psi(\tau)|\Psi_T\rangle} \tag{33}$$

The true operator expectation value can approximately be written in terms of mixed expectation values [33] as

$$\langle\mathcal{O}(\tau)\rangle \approx 2\,\langle\mathcal{O}(\tau)\rangle_{\text{mixed}} - \langle\mathcal{O}\rangle_T\,, \tag{34}$$

where

$$\langle\mathcal{O}\rangle_T = \frac{\langle\Psi_T|\,\mathcal{O}\,|\Psi_T\rangle}{\langle\Psi_T|\Psi_T\rangle} \tag{35}$$

is the variational expectation value. For the Hamiltonian and operators that commute with the Hamiltonian the mixed expectation value is exactly the true expectation value for large time step. This can be seen directly with the Hamiltonian by splitting the Green's function up, to be used on either side of the Hamiltonian.

$$\lim_{\tau\to\infty}\langle H\rangle_{\text{mixed}} = \frac{\langle\Psi_T|\,e^{-H\tau/2}He^{-H\tau/2}\,|\Psi_T\rangle}{\langle\Psi_T|\,e^{-H\tau/2}e^{-H\tau/2}\,|\Psi_T\rangle} = E_0 \tag{36}$$

The nuclear wave function is antisymmetric and will change sign as particle interact and exchange. As a result the oscillatory nature of the wave function requires positive and negative terms to cancel in the integral. Very accurate calculations must be done to accurately calculate these cancellations, and as a result very large uncertainties can be obtained. One approximate solution to this is the fixed-node approximation [34]. The basic idea is that the trial wave function defines a nodal surface that is zero at the surface and changes sign across the surface. The wave functions are not allowed to cross the nodal surface. This maintains the upper bound principle of VMC, and is exact if the trial wave function, from which the nodal surface is defined, is exactly the ground state. This method assumes

that the wave function is real, which is usually not the case with spin-isospin interactions. A generalization called the constrained path method works for real and complex wave functions alike [35]. The general idea is that walker configurations that have negative or zero overlap with the propagated wave function are discarded. This is only an approximate approach that depends on the choice of $\Psi_T(\mathbf{R})$ and does not guarantee an upper bound on the energy. To this day there is active research looking for efficient ways to solve the Fermi-sign problem in many-body quantum systems. In practice we follow the method used in [36] by using the real part of the trial wave function as the importance function and setting the weight to zero for any configuration whose overlap with the propagated wave function is zero or negative. This guarantees that the weights will be real and positive.

The constraint gives a non-exact result, however better convergence to the exact answer can be obtained by generating a set of good configurations with the constraint and then releasing the constraint for typically 20 to 40 steps to calculate the energy. Small systems, $A \leq 4$, will often converge before the statistical error overwhelms the signal. For larger systems an exponential extrapolation is typically used to determine the final energy as in [33].

The DMC algorithm can generally be written as follows.

1. Generate a set of random walkers. These are typically from the results of a VMC calculation, which has no constraint and provides an upper bound in the energy.
2. For each walker propose a move, $\mathbf{R}' = \mathbf{R} + \chi$, where χ is a vector of random numbers from the shifted Gaussian $\exp\left(\frac{m}{2\hbar^2\Delta\tau}\left(\mathbf{R}' - \mathbf{R} + 2\frac{\nabla\Psi_I(\mathbf{R}')}{\Psi_I(\mathbf{R}')}\right)^2\right)$.
3. For each walker calculate the weight $w(\mathbf{R}') = \exp\left(-\left(\frac{E_L(\mathbf{R}')+E_L(\mathbf{R})}{2} - E_0\right)\Delta\tau\right)$.
4. Do branching.
5. Calculate and collect the observables and uncertainties needed and increase the imaginary time by $\Delta\tau$.
6. Repeat steps 2 through 5 until the uncertainties are small enough.

Good reviews of this method can be found in Refs. [32] and [13]. DMC only accounts for spin-isospin independent Hamiltonians, unlike Green's function Monte Carlo (GFMC) and auxiliary field diffusion Monte Carlo (AFDMC) which follow DMC for sampling spatial states but use two different methods to sample spin-isospin states. For each set of spatial integrals there is a sum over all of the spin and isospin states. GFMC evaluates this sum explicitly. This is inefficient as the number of spin states scales as

$$\frac{A!}{Z!(A-Z)!}2^A \tag{37}$$

where A is the number of nucleons and Z is the number of protons. The number of states and the number of operators required for the trial wave function increase exponentially as the number of nucleons increases. To date, the largest nuclei that can be calculated with GFMC is ^{12}C [37, 38, 39]. AFDMC was developed as an alternative to the explicit sum over spin-isospin states that GFMC performs.

2.5 Auxiliary Field Diffusion Monte Carlo

To overcome the exponentially large number of spin-isospin states that have to be summed in GFMC, AFDMC was developed in 1999 [14] to sample spin and isospin states and, in analogy to moving the position of each walker, rotate the spin and isospin of each walker. The walkers are defined by the three spatial positions and amplitude for each particle to be in each of the four possible spin-isospin states $|s\rangle = |p\uparrow, p\downarrow, n\uparrow, n\downarrow\rangle$. The Hamiltonian can then be broken up into spin-isospin independent H_{SI} and spin-isospin dependent H_{SD} parts. The spin-isospin dependent part only comes from the potential and can be written as V_{SD}. The propagator can be broken up to have the old propagator used in DMC, which is independent of spin and isospin, and a spin-isospin dependent piece.

$$G(\mathbf{R}'S', \mathbf{R}S, \tau) = \langle \mathbf{R}' | \, e^{-(H-E_0)\tau} \, | \mathbf{R} \rangle \, G_{SD}(\mathbf{R}'S', \mathbf{R}S, \tau) \tag{38}$$

where the spin-isospin dependent part of the propagator is

$$G_{SD}(\mathbf{R}'S', \mathbf{R}S, \Delta\tau) = \langle \mathbf{R}'S' | \, e^{-V_{SD}\Delta\tau} \, | \mathbf{R}S \rangle \, . \tag{39}$$

The spin-isospin dependent part of the potential can be written as

$$V_{SD} = \sum_{p=2}^{M} \sum_{i<j} v_p(r_{ij}) \mathcal{O}^p_{ij}, \tag{40}$$

where M is the number of operators (e.g. $M = 6$ for the AV6′ potential or $M = 18$ for the Argonne AV18 two-body potential [40]). In this study I have used the standard AV6′ potential which includes the operators $\boldsymbol{\sigma}_i \cdot \boldsymbol{\sigma}_j$, $\boldsymbol{\tau}_i \cdot \boldsymbol{\tau}_j$, $\boldsymbol{\sigma}_i \cdot \boldsymbol{\sigma}_j \boldsymbol{\tau}_i \cdot \boldsymbol{\tau}_j$, S_{ij} and $S_{ij}\boldsymbol{\tau}_i \cdot \boldsymbol{\tau}_j$, where $S_{ij} = 3\boldsymbol{\sigma}_i \cdot \hat{r}_{ij} \boldsymbol{\sigma}_j \cdot \hat{r}_{ij} - \boldsymbol{\sigma}_i \cdot \boldsymbol{\sigma}_j$. Here the $\boldsymbol{\sigma}_\mathbf{i}$ and $\boldsymbol{\tau}_\mathbf{i}$ operators are the Pauli matrices applied to spin and isospin of the i-th particle respectively.

AFDMC samples the spin and isospin states by expressing the operators in terms of squared single-particle particle operators which are transformed via the Hubbard-Stratanovich transformation. This can be done if the operators are expressed in the more convenient form

$$V_{SD} = \frac{1}{2} \sum_{i,\alpha,j,\beta} \sigma_{i,\alpha} A^{\sigma}_{i,\alpha,j,\beta} \sigma_{j,\beta} + \frac{1}{2} \sum_{i,\alpha,j,\beta} \sigma_{i,\alpha} A^{\sigma\tau}_{i,\alpha,j,\beta} \sigma_{j,\beta} \boldsymbol{\tau}_i \cdot \boldsymbol{\tau}_j + \frac{1}{2} \sum_{i,j} A^{\tau}_{i,j} \boldsymbol{\tau}_i \cdot \boldsymbol{\tau}_j, \tag{41}$$

where we have defined new A matrices. The A matrices are written in terms of the $v_p(r_{ij})$ functions above. For example the simplest matrix is the $A^{\tau}_{i,j}$ matrix which can be shown to be $A^{\tau}_{i,j} = v_\tau(r_{ij})$. There is a factor of one half in Eq. 41 because the sums go over all i and j particles instead of pairs for which $i < j$. These matrices are zero when $i = j$ and they are symmetric. We can also write these matrices in terms of their eigenvalues and eigenvectors.

$$\sum_{j,\beta} A^{\sigma}_{i,\alpha,j,\beta} \psi^{\sigma}_{n,j,\beta} = \lambda^{\sigma}_n \psi^{\sigma}_{n,i,\alpha} \tag{42}$$

$$\sum_{j,\beta} A^{\sigma\tau}_{i,\alpha,j,\beta} \psi^{\sigma\tau}_{n,j,\beta} = \lambda^{\sigma\tau}_n \psi^{\sigma\tau}_{n,i,\alpha} \tag{43}$$

$$\sum_{j} A^{\tau}_{i,j} \psi^{\tau}_{n,j} = \lambda^{\tau}_n \psi^{\tau}_{n,i} \tag{44}$$

Written in terms of these eigenvalues and eigenvectors the potential can be written as

$$V_{SD} = \frac{1}{2}\sum_{n=1}^{3A}\left(O_n^\sigma\right)^2\lambda_n^\sigma + \frac{1}{2}\sum_{\alpha=1}^{3}\sum_{n=1}^{3A}\left(O_{n\alpha}^{\sigma\tau}\right)^2\lambda_n^{\sigma\tau} + \frac{1}{2}\sum_{\alpha=1}^{3}\sum_{n=1}^{A}\left(O_{n\alpha}^{\tau}\right)^2\lambda_n^{\tau}, \tag{45}$$

where the operators are given by

$$\begin{aligned} O_n^\sigma &= \sum_{j,\beta}\sigma_{j,\beta}\psi_{n,j,\beta}^\sigma \\ O_{n\alpha}^{\sigma\tau} &= \sum_{j,\beta}\tau_{j,\alpha}\sigma_{j,\beta}\psi_{n,j,\beta}^{\sigma\tau} \\ O_{n\alpha}^{\tau} &= \sum_{j}\tau_{j,\alpha}\psi_{n,j}^{\tau}. \end{aligned} \tag{46}$$

These operators in the propagator now have the effect of rotating the spinors, analogous to diffusing the walkers in space. To reduce the order of the operators in the propagator from quadratic to linear we use the Hubbard-Stratanovich transformation.

$$e^{-\frac{1}{2}\lambda O^2} = \frac{1}{\sqrt{2\pi}}\int dx e^{-\frac{x^2}{2}+\sqrt{-\lambda}xO} \tag{47}$$

The variable x is called an auxiliary field. Using the fact that there are $3A$ O_n^σ operators, $9A$ $O_{n\alpha}^{\sigma\tau}$ operators and $3A$ $O_{n\alpha}^{\tau}$ operators, for a total of $15A$ operators, and by using the Hubbard-Stratanovich transformation we can write the spin-isospin dependent part of the propagator as

$$G_{SD}(\mathbf{R}'S', \mathbf{R}S, \Delta\tau) = \langle \mathbf{R}'S'| \prod_{n=1}^{15A}\frac{1}{\sqrt{2\pi}}\int dx_n e^{-\frac{x_n^2}{2}} e^{\sqrt{-\lambda_n\Delta\tau}x_n O_n} |\mathbf{R}S\rangle . \tag{48}$$

The spinors are rotated based on auxiliary fields sampled from the Gaussian with unit variance in Eq. 48. The sampling of the auxiliary fields is done in exactly the same way as the sampling of the spatial walkers in DMC, with the Markov chain Metropolis algorithm. Each sampled auxiliary field depends only on the previous sample and no more history than that.

Importance sampling can be included in the Auxiliary Field sampling in a similar way as described before with DMC. However, in practice it is done as follows. The $\Delta\mathbf{R}$ and Δx_n are sampled by symmetric Gaussians and so the probability of $\Delta\mathbf{R}$ and $-\Delta\mathbf{R}$, and Δx_n and $-\Delta x_n$ are the same. As a result the weight for the four possible combinations are sampled as

$$w_1 = \frac{\langle\Psi_I|\mathbf{R}+\Delta\mathbf{R}, S'(x_n)\rangle}{\langle\Psi_I|\mathbf{R}S\rangle} e^{(-V_{SI}(\mathbf{R}+\Delta\mathbf{R})-E_0)\Delta\tau} \tag{49}$$

$$w_2 = \frac{\langle\Psi_I|\mathbf{R}-\Delta\mathbf{R}, S'(x_n)\rangle}{\langle\Psi_I|\mathbf{R}S\rangle} e^{(-V_{SI}(\mathbf{R}-\Delta\mathbf{R})-E_0)\Delta\tau} \tag{50}$$

$$w_3 = \frac{\langle\Psi_I|\mathbf{R}+\Delta\mathbf{R}, S'(-x_n)\rangle}{\langle\Psi_I|\mathbf{R}S\rangle} e^{(-V_{SI}(\mathbf{R}+\Delta\mathbf{R})-E_0)\Delta\tau} \tag{51}$$

$$w_4 = \frac{\langle\Psi_I|\mathbf{R}-\Delta\mathbf{R}, S'(-x_n)\rangle}{\langle\Psi_I|\mathbf{R}S\rangle} e^{(-V_{SI}(\mathbf{R}-\Delta\mathbf{R})-E_0)\Delta\tau}, \tag{52}$$

and the sample with the largest weight is used. The weight for the chosen configuration, which is used for branching, is the average of the four weights

$$W = \frac{1}{4}\sum_{n=1}^{4} w_n. \tag{53}$$

2.6 Hamiltonian

One of the difficulties in many-body nuclear physics is finding an accurate Hamiltonian that is easy to calculate with the method you have selected. For QMC methods the Hamiltonian must be in configuration space and it must be local. Small degrees of non-locality can be addressed [12, 41]. Also, the nuclear physics Hamiltonian must be able to account for 2-body and 3-body interactions. The most generic form for the nuclear Hamiltonian then takes the form

$$H = -\frac{\hbar^2}{2m}\sum_i \nabla_i^2 + \sum_{i<j} v_{ij} + \sum_{i<j<k} V_{ijk} + \dots. \tag{54}$$

In principle there could be higher order terms included the in practice the two-nucleon NN interaction v_{ij} and the three-nucleon interaction (TNI) V_{ijk} are the only terms included as the importance of an n-nuclear potential decreases as n increases. Calculations with only NN potentials will often underbind nuclei with $A > 2$ and it has been shown that the inclusion of the TNI interaction improves this underbinding as well as level ordering in the excitation spectra of nuclei. This improvement has been shown in GFMC [42] as well as other methods such as the no-core shell model [43].

The NN potential takes the form

$$v_{ij} = \sum_{p=1}^{M} v_p(\mathbf{r}_{ij})\mathcal{O}_{ij}^p, \tag{55}$$

where M is the number of operators begin used. Two-nucleon potentials are often fit to NN scattering data and several very accurate models have been developed including the Nijmengen [44, 45], CD-Bonn [46, 47], and Argonne $v18$ (AV18) potentials [40, 27]. The Argonne potential is one of the most accurate and will be used in this work. The AV18 potential has 18 operators coming from one- and two-pion exchange as well as phenomenological sources. Often a subset of the AV18 potential is used, e.g. AV4′, AV6′, AV8′ or AV14′. These AVn′ potentials have kept only the top n most important terms and are refit to scattering data at that level. A study of the successive importance of these terms up to $n = 8$ compared with the full AV18 with and without three-nucleon potentials is given in [48]. The operators of the AV18 potential are

$$\mathcal{O}_{ij}^{p=1,8} = [1, \boldsymbol{\sigma}_i\cdot\boldsymbol{\sigma}_j, S_{ij}, \mathbf{L}\cdot\mathbf{S}] \otimes [1, \boldsymbol{\tau}_i\cdot\boldsymbol{\tau}_j], \tag{56}$$

$$\mathcal{O}_{ij}^{p=9,14} = \left[\mathbf{L}^2, \mathbf{L}^2\boldsymbol{\sigma}_i\cdot\boldsymbol{\sigma}_j, (\mathbf{L}\cdot\mathbf{S})^2\right] \otimes [1, \boldsymbol{\tau}_i\cdot\boldsymbol{\tau}_j], \tag{57}$$

$$\mathcal{O}_{ij}^{p=15,18} = \left[T_{ij}, \boldsymbol{\sigma}_i\cdot\boldsymbol{\sigma}_j T_{ij}, S_{ij}T_{ij}, \tau_i^2+\tau_j^2\right], \tag{58}$$

where the tensor term is $S_{ij} = 3\boldsymbol{\sigma}_i\cdot\hat{r}_{ij}\boldsymbol{\sigma}_j\cdot\hat{r}_{ij} - \boldsymbol{\sigma}_i\cdot\boldsymbol{\sigma}_j$, the $\mathbf{L}\cdot\mathbf{S}$ term is the spin-orbit term, and the $T_{ij} = 3\tau_i^2\tau_j^2 - \boldsymbol{\tau}_i\cdot\boldsymbol{\tau}_j$ is the isotensor term.

In this work the AV6′ potential is used, which includes all of the same operators as AV8′ except for those including the spin-orbit terms, $[1, \boldsymbol{\sigma}_i \cdot \boldsymbol{\sigma}_j, S_{ij}] \otimes [1, \boldsymbol{\tau}_i \cdot \boldsymbol{\tau}_j]$. The functions multiplying the AV6′ operators are shown in figure 3.

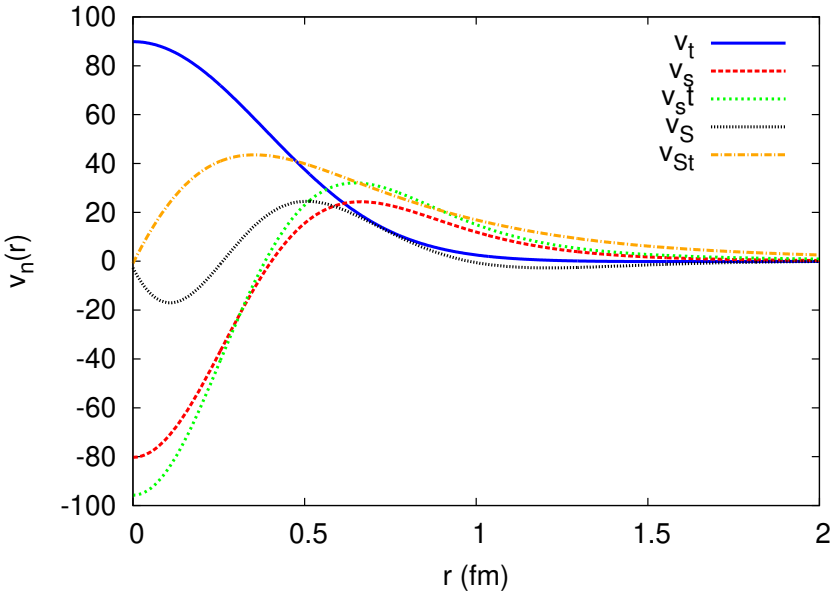

Figure 3: The functions multiplying the AV6′ operators as a function of nucleon separation. The central operator is excluded to show the spin-isospin terms with better detail. The v_s represents the spin operators, v_t the isospin operators, v_{st} the spin-isospin operators, v_S the tensor, and v_{St} the tensor-isospin operators.

The AV6′ can be broken up in Cartesian coordinates including 39 operators, 3 from τ, 9 from σ, and 27 from $\sigma\tau$ terms. This can be done by writing the potential in the form

$$\sum_p v_p(\mathbf{r}_{ij})\mathcal{O}^p_{ij} = v_1(\mathbf{r}_{ij}) + \sum_\alpha \boldsymbol{\tau}_{i\alpha} A^\tau_{ij} \boldsymbol{\tau}_{j\alpha} + \sum_{\alpha,\beta} \boldsymbol{\sigma}_{i\alpha} A^\sigma_{ij} \boldsymbol{\sigma}_{j\beta} + \sum_{\alpha,\beta,\gamma} \boldsymbol{\sigma}_{i\alpha}\boldsymbol{\tau}_{i\gamma} A^{\sigma\tau}_{ij} \boldsymbol{\sigma}_{j\beta}\boldsymbol{\tau}_{j\gamma}, \tag{59}$$

where the matrices are given by

$$A^\tau_{ij} = v_2(\mathbf{r}_{ij}), \tag{60}$$
$$A^\sigma_{ij} = v_3(\mathbf{r}_{ij})\delta_{\alpha\beta} + v_5(\mathbf{r}_{ij})(3\hat{r}^\alpha_{ij}\hat{r}^\beta_{ij} - \delta_{\alpha\beta}), \tag{61}$$
$$A^{\sigma\tau}_{ij} = v_5(\mathbf{r}_{ij})\delta_{\alpha\beta} + v_6(\mathbf{r}_{ij})(3\hat{r}^\alpha_{ij}\hat{r}^\beta_{ij} - \delta_{\alpha\beta}). \tag{62}$$

This is a simple way to break up the AV6′ potential but a more efficient breakup can be used in which only 15 operators are needed. This is achieved by using $\hat{r}_{ij}$ as the first basis function and then using two additional orthogonal basis functions. This reduces the $\hat{r}^\alpha_{ij}\hat{r}^\beta_{ij}$ term in the matrices to $\delta_{\alpha\beta}$. This potential can then be written as

$$\sum_p v_p(\mathbf{r}_{ij})\mathcal{O}^p_{ij} = v_1(\mathbf{r}_{ij}) + \sum_\alpha \boldsymbol{\tau}_{i\alpha} A^\tau_{ij} \boldsymbol{\tau}_{j\alpha} + \sum_{\alpha} \boldsymbol{\sigma}_{i\alpha} A^\sigma_{ij} \boldsymbol{\sigma}_{j\alpha} + \sum_{\alpha,\gamma} \boldsymbol{\sigma}_{i\alpha}\boldsymbol{\tau}_{i\gamma} A^{\sigma\tau}_{ij} \boldsymbol{\sigma}_{j\alpha}\boldsymbol{\tau}_{j\gamma}, \tag{63}$$

where the matrices are given by

$$A^{\tau}_{ij} = v_2(\mathbf{r}_{ij}), \tag{64}$$
$$A^{\sigma}_{ij} = v_3(\mathbf{r}_{ij}) + 2v_5(\mathbf{r}_{ij}), \tag{65}$$
$$A^{\sigma\tau}_{ij} = v_5(\mathbf{r}_{ij}) + 2v_6(\mathbf{r}_{ij}), \tag{66}$$

where it is easy to see that there are 3 τ, 3 σ, and 9 $\sigma\tau$ terms for a total of 15 operators in this basis.

Calculations with $A \leq 2$ are well described by the NN potentials, however for any system with $A \geq 3$ the 3-nucleon force is needed to accurately describe the system. The phenomenological 3-nucleon forces that are typically employed in AFDMC calculations are the older Urbana and newer Illinois potentials. The Urbana IX (UIX) potential is built using the two-pion three-nucleon interaction, which can be written as

$$\begin{aligned} V_{2\pi 3N} = \sum_{\text{cycl.}} & A_{2\pi}\{\boldsymbol{\tau}_1 \cdot \boldsymbol{\tau}_2, \boldsymbol{\tau}_1 \cdot \boldsymbol{\tau}_3\}\{(S_{12}T(\mathbf{r}_{12}) + \boldsymbol{\sigma}_1 \cdot \boldsymbol{\sigma}_2 Y(\mathbf{r}_{12})), (S_{13}T(\mathbf{r}_{13}) + \boldsymbol{\sigma}_1 \cdot \boldsymbol{\sigma}_3 Y(\mathbf{r}_{13}))\} \\ & + C_{2\pi}\left[\boldsymbol{\tau}_1 \cdot \boldsymbol{\tau}_2, \boldsymbol{\tau}_1 \cdot \boldsymbol{\tau}_3\right]\left[(S_{12}T(\mathbf{r}_{12}) + \boldsymbol{\sigma}_1 \cdot \boldsymbol{\sigma}_2 Y(\mathbf{r}_{12})), (S_{13}T(\mathbf{r}_{13}) + \boldsymbol{\sigma}_1 \cdot \boldsymbol{\sigma}_3 Y(\mathbf{r}_{13}))\right] \\ & + B(\mathbf{r}_{12}, \mathbf{r}_{13})\{\boldsymbol{\tau}_1 \cdot \mathbf{r}_2, \boldsymbol{\tau}_1 \cdot \boldsymbol{\tau}_3\}\{(S_{12} + \boldsymbol{\sigma}_1 \cdot \boldsymbol{\sigma}_2), (S_{13} + \boldsymbol{\sigma}_1 \cdot \boldsymbol{\sigma}_3)\}, \end{aligned} \tag{67}$$

where the sum is a cyclic sum over 1, 2, and 3. The { , } and [,] are anticommutators and commutators and the $Y(r)$ and $Y(r)$ are the radial Yukawa and one-pion exchange interactions as described in [28],

$$Y(r) = \frac{e^{-\mu r}}{\mu r} Y_{\text{cut}}(r) \tag{68}$$
$$T(r) = \left(1 + \frac{3}{\mu r} + \frac{3}{\mu^2 r^2}\right) \frac{e^{-\mu r}}{\mu r} T_{\text{cut}}(r), \tag{69}$$

where $Y_{\text{cut}}(r)$ and $T_{\text{cut}}(r)$ are the cutoff functions for the Yukawa and one-pion exchange terms respectively. The $B(\mathbf{r}_{12}, \mathbf{r}_{13})$ term comes from πN s-wave scattering. The UIX potential is fit to the ground states of ^{3}H and ^{4}He. For details about the construction and results obtained with this potential I refer the reader to [28, 49, 33].

The Illinois-7 (IL7) potential [29] contains two-pion three-nucleon interactions in both the s-wave and p-wave, as well as a three-pion exchange and three-nucleon contact interactions. The IL7 potential has been fit to the low-lying spectra of nuclei with $A = 3$ to nuclei with $A = 10$. These phenomenological potentials have been used to calculate many properties of light nuclei with high accuracy using both the GFMC and AFDMC methods.

Despite the accuracy of these potentials they have little direct connection to the underlying theory of QCD. In recent years a set of nuclear potentials has been developed from a chiral effective field theory (χEFT) framework that can be used with nuclear QMC methods such as GFMC and AFDMC [30, 50]. These potentials are local up the next-to-next-to leading order (N^{2}LO) and so QMC calculations can use potentials up to this order. Good results using these potentials have been obtained with both GFMC [51] and AFDMC [25].

All calculations here have been done with the AV6$'$ potential to reduce computation requirements as well as to better focus on the improvements made by improved wave functions.

It would be straightforward to do any of these calculations with the three-nucleon and the χEFT potentials.

3 Trial Wave Function

An accurate trial wave function can drastically improve the accuracy of a variational QMC method such as VMC and AFDMC. Most highly accurate trial wave functions are computationally intractable and are never implemented in QMC methods. In addition to being accurate and computationally tractable a good wave function must satisfy known physical properties such as cluster decomposition as well as having an overall antisymmetry with respect to particle exchange due to the spin-1/2 property of nucleons.

Cluster decomposition arises from the physical intuition that the wave function of two separate, non-interacting systems, A and B as in Figure 4, can be written as the outer product of their respective wave functions. If a system is not cluster decomposable unphysical

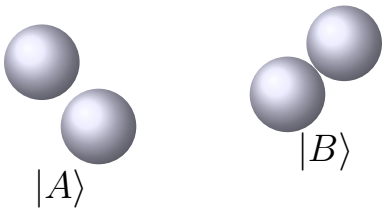

Figure 4: Two non interacting systems A and B, whose composite wave function is the product $|A+B\rangle = |A\rangle\,|B\rangle$.

correlations between non-interacting systems can occur.

The second property is that the wave function be antisymmetric overall. Since nucleons are fermions and the only degrees of freedom used in these calculations the product of different pieces of the wave function must be antisymmetric. Recent work in QMC has successfully included bosonic degrees of freedom such as pions [52], however that is not the case in this work.

3.1 Slater Determinant

One of the simplest wave functions that satisfies the two properties specified above is the Slater determinant. The Slater determinant has been the starting place for a variety of many-body calculations in nuclear and condensed matter physics alike. In condensed matter the many-body wave functions will often be written in terms of a sum of weighted Slater determinants, where some methods have been able to use a sum of up to 2 billion determinants [53, 54]. In nuclear physics a single determinant is often used for closed shell calculations and a sum of a small number of weighted determinants is used for open shell systems. For small to medium mass open-shell nuclei on the order of 10 or 100 determinants are often used. A Slater determinant is an antisymmetrized product of single particle, non-interacting, wave

functions

$$\Psi_{SD}(\mathbf{R},S)=\mathcal{A}\left[\phi_1(\mathbf{r}_1)\phi_2(\mathbf{r}_2)\dots\phi_A(\mathbf{r}_A)\right]=\begin{vmatrix}\phi_1(\mathbf{r}_1) & \phi_1(\mathbf{r}_2) & \dots & \phi_1(\mathbf{r}_A)\\ \phi_2(\mathbf{r}_1) & \phi_2(\mathbf{r}_2) & \dots & \phi_2(\mathbf{r}_A)\\ \vdots & \vdots & \ddots & \vdots\\ \phi_K(\mathbf{r}_1) & \phi_K(\mathbf{r}_2) & \dots & \phi_K(\mathbf{r}_A)\end{vmatrix}, \tag{70}$$

where $\mathbf{R}$ and S are the spatial and spin coordinates of the walkers, $\mathcal{A}$ is the antisymitrization operator, and the $\phi_i(\mathbf{r}_j)$ are the overlap of the walker positions with the model single particle states, $\langle\mathbf{r}_j|\phi_i\rangle$. The single particle model states are made up of a radial and spin, iso-spin dependent parts,

$$\phi_k=\Phi_{nj}\left[C^{j}_{c_l,m_s}Y_{l,m_l}(\hat{r}_i)\chi_s(s_i)\right]_{j,m_j}, \tag{71}$$

where Φ_{nj} is the radial part and the rest contains the spherical harmonics $Y_{l,m_l}(\hat{r}_I)$ and spin and iso-spin states where the Clebsch-Gordan coefficients ensure the correct j and m_j quantum numbers, and the different states are given by the index k. To accurately describe the wave function of an open shell nuclei each state with the correct total angular momentum, parity J^π, and isospin T is included as a separate Slater determinant.

$$\langle\mathbf{R}S|\Phi\rangle_{J^\pi,T}=\sum_n c_n D\{\phi_k(\mathbf{r}_i,s_i)\} \tag{72}$$

Here the c_n coefficients are variational parameters used to minimize the energy given a set of possible state configurations. One of the simplest examples of an open shell nuclei would be ^{6}He whose ground state is a $J^\pi=0^+$ state. The two protons and two of the neutrons could be in the full $(1S_{1/2})^2$ shell while the two remaining neutrons could be in the $(1P_{3/2})^2$ shell with their $m_j=\pm3/2,\pm1/2$ values being equal and opposite to ensure that $J=0$. This state has two possible determinants. Other possible configurations for the two remaining neutrons would be $(1P_{1/2})^2$ with one possible determinant, $(1D_{5/2})^2$ with three possible determinants, $(2S_{1/2})^2$ with one possible determinant and $(1D_{3/2})^2$ with two possible determinants giving a total of nine possible determinants. Notice that the two neutrons could be in a combination of S and D shells but never an S and P or D and P to ensure the parity of the state is positive. The number of determinants used for open shell nuclei will control how accurate the trial wave function is. For closed shell nuclei such as ^{4}He or ^{16}O a single Slater determinant describing the full shell configuration is sufficient.

The radial part Φ_{nj} of the single particle states are obtained as bound state solutions to the single particle Schrödinger equation with a Woods-Saxon potential wine-bottle potential.

$$v(r)=V_s\left[\frac{1}{1+e^{(r-r_s)/a_s}}+\alpha_s e^{(-r/\rho_s)^2}\right] \tag{73}$$

Here the parameters, V_s, r_s, a_s, α_s and ρ_s are variational parameters used to shape the potential to obtain a minimum in energy.

The Slater determinant is a mean-field wave function and is often used with Jastrow type short range correlations.

$$\langle\mathbf{R}S|\psi_T\rangle=\langle\mathbf{R}S|\prod_{i<j}f(r_{ij})\,|\phi\rangle_{SD} \tag{74}$$

These correlations are spin-isospin independent and depend only on the particle separation and improve upon the uncorrelated Slater determinant wave function significantly. To maintain the cluster decomposition the functions $f(r_{ij})$ must go to unity for large particle separations. In this work I have used Slater determinant wave functions with a Jastrow factor and spin-isospin dependent correlations which will be discussed in a later section.

3.2 Pfaffian Wave Function

Another wave function that obeys these properties is the paired Pfaffian wave function. This wave function was developed to describe Cooper pairs which form when, at low temperature, paired fermions, such as electrons or liquid ^{3}He, are energetically favorable to free particles [55, 56]. This idea was then expanded and used to explain superconductivity as the condensation of these bosonic cooper pairs into the ground state [57, 58]. A Pfaffian wave function was then introduced to describe these paired systems by Bouchaud *et al.* in 1988 [59].

The BCS, or Pfaffian, pairing wave function can be written as an antisymmetrized product of pairing wave functions, thus keeping the antisymmetry of the constituent fermions explicitly. That is,

$$\Psi_{BCS}(\mathbf{R}S) = \mathcal{A}\left[\phi(\mathbf{r}_1, s_1, \mathbf{r}_2, s_2)\phi(\mathbf{r}_3, s_3, \mathbf{r}_4, s_4)\ldots\phi(\mathbf{r}_{A-1}, s_{A-1}, \mathbf{r}_A, s_A)\right], \tag{75}$$

where $\mathcal{A}$ is the antisymmetrization operator, $\mathbf{r}_i$ and s_i are the walkers positions and spins, and ϕ are the pairing functions which can be separated into a spatial part, whose form is determined by the system, and a spin-isospin part, which are often written in terms of singlet and triplet states.

This wave function, like the Slater determinant, can be used with additional Jastrow-like correlations as in equation 74.

$$\langle \mathbf{R}S|\psi_T\rangle = \langle \mathbf{R}S|\prod_{i<j} f(r_{ij})\,|\phi\rangle_{BCS} \tag{76}$$

For more information and a more detailed use and description of this wave function I refer the reader to [60].

3.3 Spin-Isospin Dependent Correlations

The nuclear Hamiltonian has a strong dependence on spin and isospin, and to ensure good overlap with the trial wave function, the wave function must include spin-isospin dependent correlations. From here on I will be using the Slater determinant for the long-range part of the wave function. To improve on the Jastrow correlations in equation 74, spin-isospin dependent correlations can be included that obey the properties of cluster decomposability and overall antisymmetry.

I have come up with two such correlations, the exponentially correlated,

$$\Psi_{\exp}(\mathbf{R}, S) = \langle \mathbf{R}S|\left[\prod_{i<j} f_c(r_{ij})\right] e^{\sum_{i<j}\sum_p f_p(r_{ij})\mathcal{O}^p_{ij}}\,|\phi\rangle \tag{77}$$

and the symmetrized product wave functions,

$$\Psi_{\rm SP}(\mathbf{R},S) = \langle \mathbf{R}S| \left[\prod_{i<j} f_c(r_{ij})\right] \left[\mathcal{S}\prod_{i<j}\left(1+\sum_p f_p(r_{ij})\mathcal{O}^p_{ij}\right)\right] |\phi\rangle \,. \tag{78}$$

where the S is the symmetrization operator, the $f_c(r_{ij})$ are the same Jastrow correlations as before, and the $\mathcal{O}^p_{ij}$ are the operators from the AV6' potential, $(1, \boldsymbol{\sigma}_i\cdot\boldsymbol{\sigma}_j, S_{ij})\otimes(1,\boldsymbol{\tau}_i\cdot\boldsymbol{\tau}_j)$, where the tensor term is $S_{ij} = 3\boldsymbol{\sigma}_i\cdot\hat{r}_{ij}\boldsymbol{\sigma}_j\cdot\hat{r}_{ij} - \boldsymbol{\sigma}_i\cdot\boldsymbol{\sigma}_j$. The $f_p(r_{ij})$ functions contain variational parameters and the functional form is determined by solving a Schrödinger-type equation with the constraint that the wave function be continuous at the healing distance [61, 62].

The exponentially correlated wave function obeys cluster decomposition as long as the correlating functions, $f_p(r_{ij})$ go to zero as the particle separation increases. This dampens out unphysical long-range particle correlations between physically separated systems. Also, due to the sum over particle pairs in the exponential, no explicit symmetrization is needed.

The symmetrized product wave function, introduced by Pandharipande and Wiringa in 1979 [61], requires an explicit symmetrization and is not obviously cluster decomposable. The $f_p(r_{ij})$ functions approach zero as particle separation increases and so the additional 1 is needed to maintain cluster decomposability.

When expanded to linear order the exponential and symmetrized product correlations are identical and can be written as

$$|\psi_T\rangle_{\rm lin} = \left[\prod_{i<j} f_c(r_{ij})\right] \left(1+\sum_{i<j}\sum_p f_p(r_{ij})\mathcal{O}^p_{ij}\right) |\phi\rangle \,. \tag{79}$$

These correlations are symmetric, allowing for the full wave function to be antisymmetric, however it has lost the cluster decomposability in the approximation. This is because they take the form of summed, not a product of pair correlations. For higher orders expansions these two wave functions differ by commutation relations as well as the inclusion of additional correlation pairs. Until recently, only correlations up to linear order in the expansion were used for AFDMC calculations. Calculations for GFMC use a much better wave function, but have been limited to small nuclei up to ^{12}C. Calculations done with the AFDMC method have been slowly improving the trial wave function used, as a better wave function is surely needed to describe larger systems. In 2007 AFDMC binding energy calculations were done for ^{4}He, ^{16}O, and ^{40}Ca using only the Jastrow correlations [15]. These calculations were repeated in 2014 but with the addition of linear correlations [23] and I have plotted the respective results compared to current experimental values here for comparison. In figure 5 it is clear to see that the additional spin-isospin correlations are important for both systems larger than ^{4}He.

3.3.1 Quadratic Correlations

In this project I have included correlations up to quadratic order which includes up to 4 nucleons begin correlated at once. When expanded to quadratic order the symmetrized

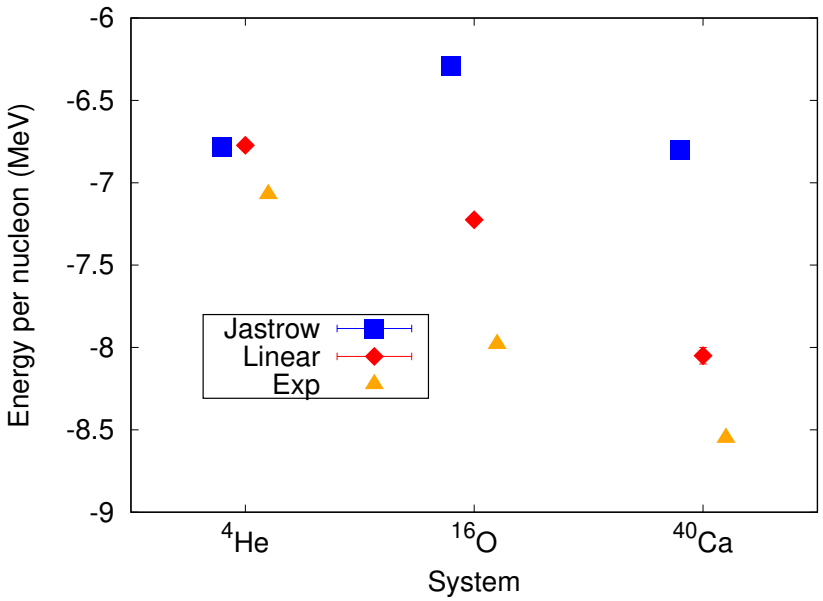

Figure 5: Binding energy calculations done with Jastrow correlations [15] compared to Jastrow plus linear spin-isospin dependent correlations [23] all compared to experimental results. All calculations were done with AFDMC and the AV6′ potential.

product wave function, equation 78, becomes

$$|\psi_T\rangle_{\rm quad} = \left[\prod_{i<j} f_c(r_{ij})\right]\left[1 + \sum_{i<j}\sum_{p} f_p(r_{ij})\mathcal{O}^p_{ij} + \frac{1}{2}\sum_{i<j}\sum_{p} f_p(r_{ij})\mathcal{O}^p_{ij}\sum_{\substack{k<l\\ ij\neq kl}}\sum_{q} f_q(r_{kl})\mathcal{O}^q_{kl}\right]|\phi\rangle\,. \tag{80}$$

The subscripts on the sums, which describe which correlations are allowed, can be hard to visualize and so these correlation diagrams are useful. All pair correlations are included in

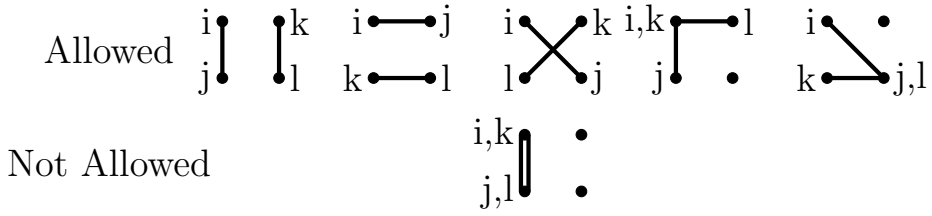

Figure 6: Diagrams used to visualize which correlations are included in the quadratic correlations in equation 80.

this wave function except pairs that are directly correlated with themselves, e.g. $\mathcal{O}_{23}\mathcal{O}_{23}$, where $\mathcal{O}_{ij}$ is a product of single particle operators such as $\boldsymbol{\sigma}_i \cdot \boldsymbol{\sigma}_j$ and $\mathcal{O}_{ij} = \mathcal{O}_{ji}$ due to the operators on different particles operating in different Hilbert spaces. For correlations where

the same particle is included twice, the correlation operators do not commute and that term must be explicitly symmetrized. Currently in equation 80 and in the code all quadratic terms are symmetrized, e.g. the correlation $\mathcal{O}_{12}\mathcal{O}_{34}$ is symmetrized as $\frac{1}{2}\left(\mathcal{O}_{12}\mathcal{O}_{34} + \mathcal{O}_{34}\mathcal{O}_{12}\right)$, even though only terms like $\mathcal{O}_{12}\mathcal{O}_{13}$ need this explicit symmetrization. This adds needless calculation time, but as I'll show, these terms don't seem to be significant and can be omitted completely.

If the exponentially correlated wave function, equation 77, is expanded in the typical way, i.e. $\exp(A) = 1 + A + \frac{1}{2}A^2 + \ldots$, then the quadratic correlations for the exponential wave function become

$$\begin{aligned} |\psi_T\rangle_{\text{exp\_quad}} = \left[\prod_{i<j} f_c(r_{ij})\right]\Bigg[1 + \sum_{i<j}\sum_{p} f_p(r_{ij})\mathcal{O}^p_{ij} \\ + \frac{1}{2}\sum_{i<j}\sum_{p} f_p(r_{ij})\mathcal{O}^p_{ij}\sum_{k<l}\sum_{q} f_q(r_{kl})\mathcal{O}^q_{kl}\Bigg]|\phi\rangle\,. \end{aligned} \tag{81}$$

Unlike the quadratic correlations derived from the symmetrized product this wave function includes all of the the terms in figure 6. There is not a large difference between these wave functions up to quadratic order and for here forward all references to quadratic correlations will refer to the expansion from the symmetrized product wave function.

Another way to include quadratic correlations is to only include terms that do not correlate the same particle twice leaving only independent pair correlations. This is the same whether you start from the exponentially correlated or the symmetrized product wave function and it can be written as

$$\begin{aligned} |\psi_T\rangle_{\text{ip}} = \left[\prod_{i<j} f_c(r_{ij})\right]\Bigg[1 + \sum_{i<j}\sum_{p} f_p(r_{ij})\mathcal{O}^p_{ij} \\ + \sum_{i<j}\sum_{p} f_p(r_{ij})\mathcal{O}^p_{ij}\sum_{k<l,\text{ip}}\sum_{q} f_q(r_{kl})\mathcal{O}^q_{kl}\Bigg]|\phi\rangle \end{aligned} \tag{82}$$

and the independent pair sum can be visualized as in figure 7. All terms where a particle is

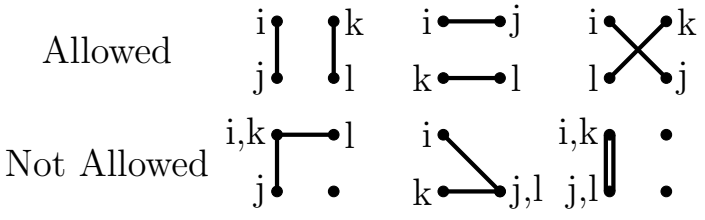

Figure 7: Diagrams used to visualize which correlations are included in the independent pair quadratic correlations in equation 82.

included twice in the correlation are ignored, as a results, all correlation operators commute and the correlations are explicitly symmetric. Neither of these correlations maintains cluster

decomposability, however an effort to build an antisymmetric and cluster decomposable wave function from the exponentially correlated wave function will be discussed later.

The energy and it's uncertainty are used to judge the convergence of a propagated wave function in QMC and so a good wave function needs to be able to reproduce known binding energies. To this end I have calculated binding energies with the linear, quadratic, and independent pair (IP) quadratic correlations derived from the symmetrized product for ^{4}He, ^{16}O, ^{40}Ca, and symmetric nuclear matter (SNM) at saturation density, $\rho_0 = 0.16$ fm^{-3}, in a period box with 28 particles. The energy per particle for nuclei is plotted in figure 8 and the specific energies can be found in table 3.3.1. Like with the addition of Jastrow

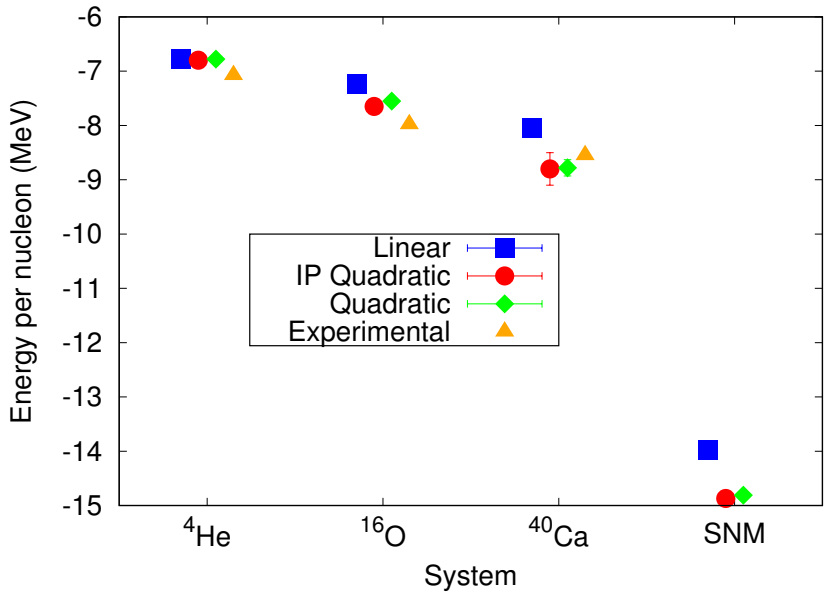

Figure 8: Energy per particle for small and medium closed shell nuclei with no Coulomb interaction with the AV6′ interaction. Each calculations was done with the linear, independent pair, and quadratic correlations. Energies are compared to experimental values where available and the statistical uncertainties are included.

System	Linear	Ind-Pair	Quadratic	Experimental
^{4}He	-6.785(10)	-6.798(8)	-6.778(8)	-7.074
^{16}O	-7.23(6)	-7.65(9)	-7.55(8)	-7.98
^{40}Ca	-8.05(8)	-8.8(3)	-8.78(15)	-8.55
SNM	-13.97(3)	-14.87(4)	-14.70(11)	

Table 1: Energy per particle calculated with no Coulomb interaction with the AV6′ interaction. Each calculations was done with the linear, independent pair, and quadratic correlations. Energies are compared to experimental values where available and the statistical uncertainties are included.

correlations in figure 5, all systems larger than ^{4}He decreased in energy with additional correlations, while the binding energy for ^{4}He was the same to within uncertainties. In

addition, the energies for all systems are identical to within uncertainties for the quadratic and IP quadratic correlations, indicating that the IP correlations capture most of the relevant physics. As a result any further references to quadratic correlations will be referring to the IP quadratic correlations, as these correlations are computationally less expensive, unless a distinction is made otherwise. The percent decrease in energy for ^{16}O and ^{40}Ca when adding linear correlations is 15% and 18% respectively. When adding quadratic correlations the energies decrease an additional 6% and 9% respectively. This indicates that each successive term in the expansion decreases in importance.

There is a significant decrease in energy with the addition of the quadratic correlations, however, there is an additional cost to calculating these additional terms. I have calculated a scaling factor, which is the ratio of times taken to calculate a given block of code, including the propagation of walkers spatial and spin components as well as the calculation of the energies, for linear compared to linear plus quadratic correlations. A scaling factor of 2 would mean that the calculation took twice as long with the quadratic correlations as it did without. The scaling factors are plotted in figure 9 and the specific values are in table 3.3.1. The

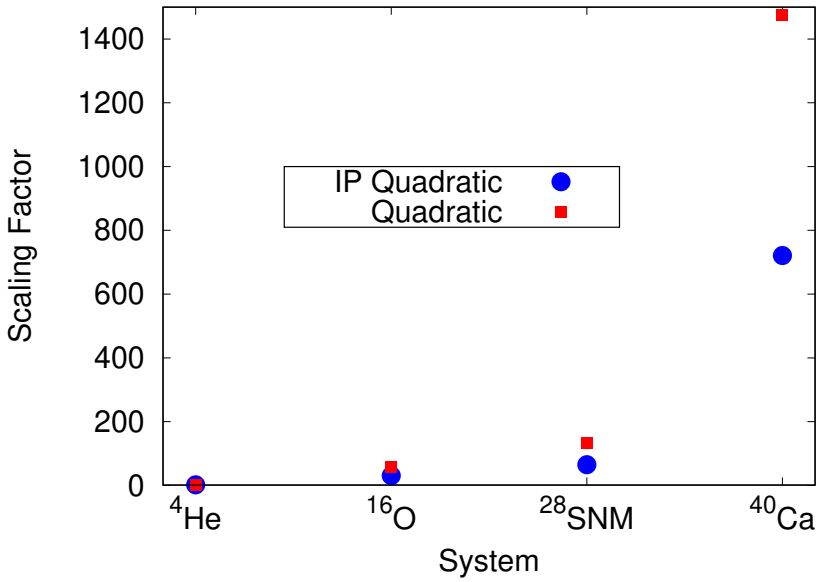

Figure 9: Scaling factors calculated as the ratio of times taken to calculate a given block of code for linear and linear plus quadratic correlations.

	^{4}He	^{16}O	SNM(28)	^{40}Ca
IP Quadratic	1.73	30.7	64.8	720.9
Quadratic	2.00	58.8	133.6	1473.9

Table 2: Same scaling factors that are calculated in figure 9.

scaling for the quadratic correlations is about twice that of the IP quadratic correlations. This is due to the explicit symmetrization that is done for each quadratic term in the quadratic correlations. This could be decreased if commuting terms were not symmetrized, however

as noted before the IP quadratic correlations seem to capture the important physics, and so all future calculations with quadratic correlations will be using the IP correlations. The IP correlations all commute and so no explicit symmetrization is needed. A typical AFDMC calculation using only linear correlations for ^{16}O with 1000 walkers takes on the order of a tens of CPU hours and a similar calculation for ^{40}Ca takes on the order of hundreds of CPU hours.

The number of quadratic terms in the IP correlations given A particles is

$$N_{\rm ip} = \frac{A(A-1)(A-2)(A-3)}{8}. \tag{83}$$

For the fully quadratic wave function the number of terms given A particles is

$$N_{\rm quad} = \frac{A(A-1)}{2}\left(\frac{A(A-1)}{2} - 1\right), \tag{84}$$

where $A(A-1)/2$ is the number of possible pairs made from A particles. If the fully quadratic correlations are not explicitly symmetrized for the IP terms then this reduces to $N_{\rm quad} - N_{\rm ip}$. In figure 10 I have plotted the number of terms for the independent pair, fully quadratic, and fully quadratic correlations without symmetrizing the IP terms.

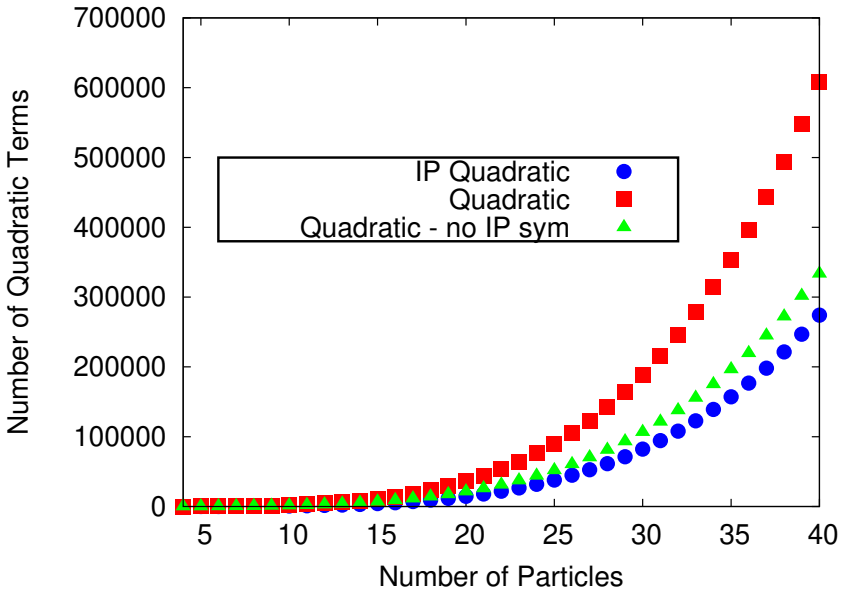

Figure 10: Number of terms in the quadratic correlations for the IP, quadratic, and quadratic correlations without explicit symmetrization of the IP terms.

In recent years efforts have been made to fit infinite matter saturation properties with microscopic nuclear interactions [63]. Calculations of energies near saturation using AFDMC have not been able to fit known saturation properties. I have done calculations of symmetric nuclear matter near saturation with and without quadratic correlations, using only the AV6′ 2-body interaction and have compared these results to known saturation properties in figure 11. Though 3N forces will surely be needed to obtain a good fit, it is clear that improved correlations are also going to be needed.

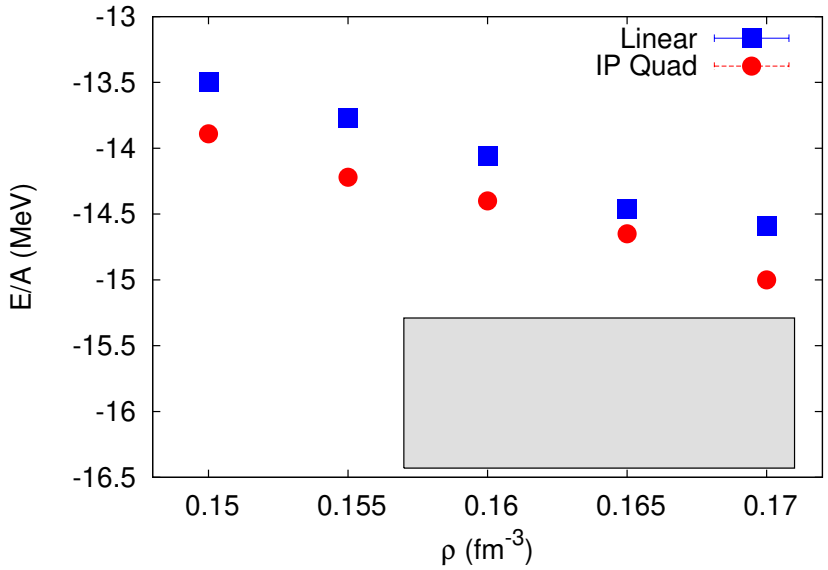

Figure 11: Energy calculations done using the AV6′ potential with linear and quadratic correlations. The gray box is the same empirical saturation region used in [63], $\rho_0 = 0.164 \pm 0.007$ fm^{-3} and $E/A = -15.86 \pm 0.57$ MeV.

3.3.2 Exponential Correlations

From the wave function using the expansion up to quadratic terms it is clear that an improved trial wave function is necessary to describe the state of larger nuclei and nuclear matter. It was also shown in the previous sections that expanding the current wave functions, Equations 77 and 78 is not an efficient method to improve the wave function, as the cost of each additional term grows exponentially. However, another option is to evaluate the full wave function using a Monte Carlo sampling. The exponential wave function is written as

$$|\Psi_T\rangle = \left[\prod_{i<j} f_c(r_{ij})\right] e^{\sum_{i<j,p} f_p(r_{ij})\mathcal{O}^p_{ij}} |\Phi\rangle \,, \tag{85}$$

which has the same operator form as the spin-isospin propagator used in AFDMC, where again, the operators are the AV6′ operators, $\boldsymbol{\sigma}_i \cdot \boldsymbol{\sigma}_j$, $\boldsymbol{\tau}_i \cdot \boldsymbol{\tau}_j$, $\boldsymbol{\sigma}_i \cdot \boldsymbol{\sigma}_j \boldsymbol{\tau}_i \cdot \boldsymbol{\tau}_j$, S_{ij} and $S_{ij}\boldsymbol{\tau}_i \cdot \boldsymbol{\tau}_j$, where $S_{ij} = 3\boldsymbol{\sigma}_i \cdot \hat{r}_{ij} \boldsymbol{\sigma}_j \cdot \hat{r}_{ij} - \boldsymbol{\sigma}_i \cdot \boldsymbol{\sigma}_j$. These operators are written in terms of squared single particle operators, allowing for the Hubbard Stratanovich transformation to express the correlations in terms of a single particle operator and integrals over auxiliary fields, which are evaluated via Monte Carlo.

The correlation functions $f_p(r_{ij})$ are written in terms of symmetric matrices

$$\exp\left(\sum_{i<j,p} f_p(r_{ij})\mathcal{O}^p_{ij}\right) = \exp\left(\frac{1}{2}\sum_{i\alpha,j\beta} \sigma_{i\alpha} A^{\sigma}_{i\alpha,j\beta} \sigma_{j\beta} + \frac{1}{2}\sum_{i\alpha,j\beta} \sigma_{i\alpha} A^{\sigma\tau}_{i\alpha,j\beta} \sigma_{j\beta} \boldsymbol{\tau}_i \cdot \boldsymbol{\tau}_j + \frac{1}{2}\sum_{i,j} A^{\tau}_{i,j} \boldsymbol{\tau}_i \cdot \boldsymbol{\tau}_j\right), \tag{86}$$

which can be written in terms of their eigenvalues and eigenvectors

$$\sum_{j\beta} A^{\sigma}_{i\alpha,j\beta}\psi^{\sigma}_{n,j\beta} = \lambda^{\sigma}_{n}\psi^{\sigma}_{n,i\alpha} \tag{87}$$

$$\sum_{j\beta} A^{\sigma\tau}_{i\alpha,j\beta}\psi^{\sigma\tau}_{n,j\beta} = \lambda^{\sigma\tau}_{n}\psi^{\sigma\tau}_{n,i\alpha} \tag{88}$$

$$\sum_{j} A^{\tau}_{i,j}\psi^{\tau}_{n,j} = \lambda^{\tau}_{n}\psi^{\tau}_{n,i}. \tag{89}$$

The correlations are then written in terms of squared single particle operators,

$$\exp\left(\sum_{i<j,p} f_p(r_{ij})\mathcal{O}^p_{ij}\right) = \exp\left(\frac{1}{2}\sum_{n=1}^{3A}\left(O^{\sigma}_{n}\right)^2\lambda^{\sigma}_{n} + \frac{1}{2}\sum_{\alpha=1}^{3}\sum_{n=1}^{3A}\left(O^{\sigma\tau}_{n\alpha}\right)^2\lambda^{\sigma\tau}_{n} + \frac{1}{2}\sum_{\alpha=1}^{3}\sum_{n=1}^{A}\left(O^{\tau}_{n\alpha}\right)^2\lambda^{\tau}_{n}\right), \tag{90}$$

where the operators are given by

$$\begin{aligned} O^{\sigma}_{n} &= \sum_{j,\beta}\sigma_{j,\beta}\psi^{\sigma}_{n,j,\beta} \\ O^{\sigma\tau}_{n\alpha} &= \sum_{j,\beta}\tau_{j,\alpha}\sigma_{j,\beta}\psi^{\sigma\tau}_{n,j,\beta} \\ O^{\tau}_{n\alpha} &= \sum_{j}\tau_{j,\alpha}\psi^{\tau}_{n,j}. \end{aligned} \tag{91}$$

This can be written in a more compact form,

$$\exp\left(\sum_{i<j,p} f_p(r_{ij})\mathcal{O}^p_{ij}\right) = \exp\left(\frac{1}{2}\sum_{n=1}^{15A}\left(O_n\right)^2\lambda^{\sigma}_{n}\right). \tag{92}$$

The Hubbard Stratanovich transformation is then used to write these as single particle operators and integrals over auxiliary fields, x_n. Ignoring commutator terms this can be written as

$$\exp\left(\frac{1}{2}\sum_{n=1}^{15A}\left(O_n\right)^2\lambda^{\sigma}_{n}\right) = \prod_{n=1}^{15A}\frac{1}{\sqrt{2\pi}}\int dx_n e^{-x_n^2/2}e^{\sqrt{\lambda_n}x_n O_n}. \tag{93}$$

The auxiliary fields are then drawn from the Gaussian distribution, $\exp\left(-x_n^2/2\right)$ and the correlations can be written as

$$\Psi_T(R,S) = \langle RS|\prod_{n=1}^{15A}\frac{1}{N}\sum_{\{x_n\}}^{N}\frac{1}{\sqrt{2\pi}}e^{\sqrt{\lambda_n}x_n O_n}\left|\Phi\right\rangle. \tag{94}$$

The $\{x_n\}$ are the set of $15A$ auxiliary fields, one for each of the different $15A$ operators.

Minimal success has been achieved with these correlations for light nuclei [64], however there are large uncertainties that make this wave function currently infeasible to use. Removing these uncertainties could make this wave function a very useful tool for nuclear QMC

as it can be systematically improved by increasing the number of samples of the auxiliary fields.

One difference between this wave function and the propagator used in AFDMC is the lack of a small time step. This wave function contains no time step and so there is no way to ensure that commutator terms will be small. Another possible issue arises when evaluating the derivative in the kinetic energy. The shifting of the walker positions causes the A matrices to be discontinuous, and thus causing large uncertainties in the calculation of the derivative.

3.3.3 Alessandro's correlations and T^2 fix to them - Maybe just do T^2 fix and apply it to exponential correlations . . . maybe don't include this at all.

References

[1] D. R. Hartree. The wave mechanics of an atom with a non-coulomb central field. part i. theory and methods. *Mathematical Proceedings of the Cambridge Philosophical Society*, 24(1):89110, 1928.

[2] V. Fock. Näherungsmethode zur lösung des quantenmechanischen mehrkörperproblems. *Zeitschrift für Physik*, 61(1):126–148, Jan 1930.

[3] J. C. Slater. A simplification of the Hartree-Fock method. *Phys. Rev.*, 81:385, 1951.

[4] J. Žofka. Application of the hartree-fock method in nuclear theory. *Czechoslovak Journal of Physics B*, 20(8):926–938, Aug 1970.

[5] Gogny, D. and Lions, P. L. Hartree-fock theory in nuclear physics. *ESAIM: M2AN*, 20(4):571–637, 1986.

[6] Petr Navrátil, Sofia Quaglioni, Ionel Stetcu, and Bruce R Barrett. Recent developments in no-core shell-model calculations. *Journal of Physics G: Nuclear and Particle Physics*, 36(8):083101, 2009.

[7] Bruce R. Barrett, Petr Navrátil, and James P. Vary. *Ab initio* no core shell model. *Prog. Part. Nucl. Phys.*, 69:131–181, 2013.

[8] G Hagen, T Papenbrock, M Hjorth-Jensen, and D J Dean. Coupled-cluster computations of atomic nuclei. *Rep. Prog. Phys.*, 77(9):096302, 2014.

[9] W.H. Dickhoff and C. Barbieri. Self-consistent Green's function method for nuclei and nuclear matter. *Prog. Part. Nucl. Phys.*, 52(2):377 – 496, 2004.

[10] V. Somà, A. Cipollone, C. Barbieri, P. Navrátil, and T. Duguet. Chiral two- and three-nucleon forces along medium-mass isotope chains. *Phys. Rev. C*, 89:061301, Jun 2014.

[11] H. Hergert, S.K. Bogner, T.D. Morris, A. Schwenk, and K. Tsukiyama. The in-medium similarity renormalization group: A novel ab initio method for nuclei. *Phys. Rep.*, 621:165–222, 2016. Memorial Volume in Honor of Gerald E. Brown.

[12] J. E. Lynn and K. E. Schmidt. Real-space imaginary-time propagators for non-local nucleon-nucleon potentials. *Phys. Rev. C*, 86:014324, Jul 2012.

[13] J. Carlson, S. Gandolfi, F. Pederiva, Steven C. Pieper, R. Schiavilla, K.E. Schmidt, and R.B. Wiringa. Quantum Monte Carlo methods for nuclear physics. *Rev. Mod. Phys.*, 87:1067, 2015.

[14] K. E. Schmidt and S. Fantoni. A quantum Monte Carlo method for nucleon systems. *Phys. Lett. B*, 446:99–103, 1999.

[15] S. Gandolfi, F. Pederiva, S. Fantoni, and K. E. Schmidt. Auxiliary field diffusion monte carlo calculation of nuclei with $a \leq 40$ with tensor interactions. *Phys. Rev. Lett.*, 99:022507, Jul 2007.

[16] D. Lonardoni, A. Lovato, Steven C. Pieper, and R. B. Wiringa. Variational calculation of the ground state of closed-shell nuclei up to $a = 40$. *Phys. Rev. C*, 96:024326, Aug 2017.

[17] S. Gandolfi, J. Carlson, S. Reddy, A. W. Steiner, and R. B. Wiringa. The equation of state of neutron matter, symmetry energy and neutron star structure. *The European Physical Journal A*, 50(2):10, Feb 2014.

[18] S. Gandolfi, J. Carlson, and Sanjay Reddy. Maximum mass and radius of neutron stars, and the nuclear symmetry energy. *Phys. Rev. C*, 85:032801, Mar 2012.

[19] I. Tews, J. Carlson, S. Gandolfi, and S. Reddy. Constraining the speed of sound inside neutron stars with chiral effective field theory interactions and observations. *The Astrophysical Journal*, 860(2):149, jun 2018.

[20] Diego Lonardoni, Alessandro Lovato, Stefano Gandolfi, and Francesco Pederiva. Hyperon puzzle: Hints from quantum monte carlo calculations. *Phys. Rev. Lett.*, 114:092301, Mar 2015.

[21] Stefano Gandolfi and Diego Lonardoni. *The EOS of Neutron Matter and the Effect of Hyperons to Neutron Star Structure.*

[22] Stefano Gandolfi, Francesco Pederiva, Stefano Fantoni, and Kevin E. Schmidt. Quantum monte carlo calculations of symmetric nuclear matter. *Phys. Rev. Lett.*, 98:102503, Mar 2007.

[23] S. Gandolfi, A. Lovato, J. Carlson, and Kevin E. Schmidt. From the lightest nuclei to the equation of state of symmetric nuclear matter with realistic nuclear interactions. *Phys. Rev. C*, 90, 2014.

[24] D. Lonardoni, J. Carlson, S. Gandolfi, J. E. Lynn, K. E. Schmidt, A. Schwenk, and X. B. Wang. Properties of nuclei up to $a = 16$ using local chiral interactions. *Phys. Rev. Lett.*, 120:122502, Mar 2018.

[25] D. Lonardoni, S. Gandolfi, J. E. Lynn, C. Petrie, J. Carlson, K. E. Schmidt, and A. Schwenk. Auxiliary field diffusion monte carlo calculations of light and medium-mass nuclei with local chiral interactions. *Phys. Rev. C*, 97:044318, Apr 2018.

[26] J.E. Lynn, I. Tews, S. Gandolfi, and A. Lovato. Quantum monte carlo methods in nuclear physics: Recent advances.

[27] R. B. Wiringa, V. G. J. Stoks, and R. Schiavilla. Accurate nucleon-nucleon potential with charge-independence breaking. *Phys. Rev. C*, 51:38–51, Jan 1995.

[28] J. Carlson, V.R. Pandharipande, and R.B. Wiringa. Three-nucleon interaction in 3-, 4- and -body systems. *Nuclear Physics A*, 401(1):59 – 85, 1983.

[29] Steven C. Pieper, V. R. Pandharipande, R. B. Wiringa, and J. Carlson. Realistic models of pion-exchange three-nucleon interactions. *Phys. Rev. C*, 64:014001, Jun 2001.

[30] E. Epelbaum, H.-W. Hammer, and Ulf-G. Meißner. Modern theory of nuclear forces. *Rev. Mod. Phys.*, 81:1773–1825, Dec 2009.

[31] A. Gezerlis, I. Tews, E. Epelbaum, S. Gandolfi, K. Hebeler, A. Nogga, and A. Schwenk. Quantum monte carlo calculations with chiral effective field theory interactions. *Phys. Rev. Lett.*, 111:032501, Jul 2013.

[32] W. M. C. Foulkes, L. Mitas, R. J. Needs, and G. Rajagopal. Quantum Monte Carlo simulations of solids. *Rev. Mod. Phys.*, 73:33–83, 2001.

[33] B. S. Pudliner, V. R. Pandharipande, J. Carlson, Steven C. Pieper, and R. B. Wiringa. Quantum monte carlo calculations of nuclei with $A \leq 7$. *Phys. Rev. C*, 56:1720–1750, Oct 1997.

[34] Jules W. Moskowitz, K. E. Schmidt, Michael A. Lee, and M. H. Kalos. A new look at correlation energy in atomic and molecular systems. ii. the application of the greens function monte carlo method to lih. *The Journal of Chemical Physics*, 77(1):349–355, 1982.

[35] R. B. Wiringa, Steven C. Pieper, J. Carlson, and V. R. Pandharipande. Quantum monte carlo calculations of $a = 8$ nuclei. *Phys. Rev. C*, 62:014001, Jun 2000.

[36] Shiwei Zhang and Henry Krakauer. Quantum monte carlo method using phase-free random walks with slater determinants. *Phys. Rev. Lett.*, 90:136401, Apr 2003.

[37] A. Lovato, S. Gandolfi, Ralph Butler, J. Carlson, Ewing Lusk, Steven C. Pieper, and R. Schiavilla. Charge form factor and sum rules of electromagnetic response functions in $^{12}\mathbf{C}$. *Phys. Rev. Lett.*, 111:092501, Aug 2013.

[38] A. Lovato, S. Gandolfi, J. Carlson, Steven C. Pieper, and R. Schiavilla. Neutral weak current two-body contributions in inclusive scattering from ^{12}C. *Phys. Rev. Lett.*, 112:182502, May 2014.

[39] A. Lovato, S. Gandolfi, J. Carlson, Steven C. Pieper, and R. Schiavilla. Electromagnetic and neutral-weak response functions of ^{4}He and ^{12}C. *Phys. Rev. C*, 91:062501, Jun 2015.

[40] R.B. Wiringa, R.A. Smith, and T.L. Ainsworth. Nucleon-nucleon potentials with and without $\Delta(1232)$ degrees of freedom. *Phys. Rev. C*, 29:1207, 1984.

[41] Joel E. Lynn. *Quantum Monte Carlo Calculations of Light Nuclei with Non-Local Potentials*. PhD thesis, Arizona State University, April 2013.

[42] Stefano Fantoni, Stefano Gandolfi, Alexey Yu. Illarionov, Kevin E. Schmidt, and Francesco Pederiva. Monte carlo approach to nuclei and nuclear matter. *AIP Conference Proceedings*, 1056(1):233–240, 2008.

[43] Petr Navrátil and W. Erich Ormand. Ab initio shell model with a genuine three-nucleon force for the p-shell nuclei. *Phys. Rev. C*, 68:034305, Sep 2003.

[44] M.M. Nagels, T.A. Rijken, and J.J. de Swart. Baryon-baryon scattering in a one-boson-exchange-potential approach. i. nucleon-nucleon sattering. *Phys. Rev. D*, 12:744–758, 1975.

[45] V. G. J. Stoks, R. A. M. Klomp, C. P. F. Terheggen, and J. J. de Swart. Construction of high-quality nn potential models. *Phys. Rev. C*, 49:2950–2962, Jun 1994.

[46] R. Machleidt, F. Sammarruca, and Y. Song. Nonlocal nature of the nuclear force and its impact on nuclear structure. *Phys. Rev. C*, 53:R1483–R1487, Apr 1996.

[47] R. Machleidt. High-precision, charge-dependent bonn nucleon-nucleon potential. *Phys. Rev. C*, 63:024001, Jan 2001.

[48] R. B. Wiringa and Steven C. Pieper. Evolution of nuclear spectra with nuclear forces. *Phys. Rev. Lett.*, 89:182501, Oct 2002.

[49] B. S. Pudliner, A. Smerzi, J. Carlson, V. R. Pandharipande, Steven C. Pieper, and D. G. Ravenhall. Neutron drops and skyrme energy-density functionals. *Phys. Rev. Lett.*, 76:2416–2419, Apr 1996.

[50] R. Machleidt and D.R. Entem. Chiral effective field theory and nuclear forces. *Physics Reports*, 503(1):1 – 75, 2011.

[51] J. E. Lynn, J. Carlson, E. Epelbaum, S. Gandolfi, A. Gezerlis, and A. Schwenk. Quantum monte carlo calculations of light nuclei using chiral potentials. *Phys. Rev. Lett.*, 113:192501, Nov 2014.

[52] Lucas Madeira, Alessandro Lovato, Francesco Pederiva, and Kevin E. Schmidt. Quantum monte carlo formalism for dynamical pions and nucleons. *Phys. Rev. C*, 98:034005, Sep 2018.

[53] B. Huron, J. P. Malrieu, and P. Rancurel. Iterative perturbation calculations of ground and excited state energies from multiconfigurational zerothorder wavefunctions. *The Journal of Chemical Physics*, 58(12):5745–5759, 1973.

[54] Junhao Li, Matthew Otten, Adam A. Holmes, Sandeep Sharma, and C. J. Umrigar. Fast semistochastic heat-bath configuration interaction. *The Journal of Chemical Physics*, 149(21):214110, 2018.

[55] Leon N. Cooper. Bound electron pairs in a degenerate fermi gas. *Phys. Rev.*, 104:1189–1190, Nov 1956.

[56] Anthony J. Leggett. A theoretical description of the new phases of liquid ^{3}He. *Rev. Mod. Phys.*, 47:331–414, Apr 1975.

[57] J. Bardeen, L. N. Cooper, and J. R. Schrieffer. Microscopic theory of superconductivity. *Phys. Rev.*, 106:162–164, Apr 1957.

[58] J. Bardeen, L. N. Cooper, and J. R. Schrieffer. Theory of superconductivity. *Phys. Rev.*, 108:1175–1204, Dec 1957.

[59] Bouchaud, J.P., Georges, A., and Lhuillier, C. Pair wave functions for strongly correlated fermions and their determinantal representation. *J. Phys. France*, 49(4):553–559, 1988.

[60] Lucas Madeira. *Quantum Monte Carlo Studies of Strongly Interacting Fermionic Systems*. PhD thesis, Arizona State University, June 2018.

[61] V. R. Pandharipande and R. B. Wiringa. Variations on a theme of nuclear matter. *Rev. Mod. Phys.*, 51:821–861, Oct 1979.

[62] V. R. Pandharipande and K. E. Schmidt. Variational calculations of simple bose systems. *Phys. Rev. A*, 15:2486–2495, Jun 1977.

[63] C. Drischler, K. Hebeler, and A. Schwenk. Chiral interactions up to next-to-next-to-next-to-leading order and nuclear saturation. *Phys. Rev. Lett.*, 122:042501, Jan 2019.

[64] M. Y. Bouadani. *Monte Carlo calculations of pion condensate in highly dense neutron matter and a new auxiliary fields correlated wavefunction*. PhD thesis, Arizona State University, 2009.